UNIVERSITY OF CALIFORNIA, SAN DIEGO

Understanding Locomotor Deficits by Analysis of *Nmf9* Gene

A dissertation submitted in partial satisfaction of the requirements for the degree

Doctor of Philosophy

in

Biomedical Sciences

by

Shuxiao Zhang

Committee in charge:

Professor Bruce A. Hamilton, Chair
Professor Don W. Cleveland
Professor Michael R. Gorman
Professor Yishi Jin
Professor Binhai Zheng

2014

The Dissertation of Shuxiao Zhang is approved, and it is acceptable in quality and form for publication on microfilm and electronically:

_____

_____

_____

_____

_____

Chair

University of California, San Diego

2014

Dedication

This dissertation is dedicated to:

My group of close friends, who were there to cheer me on through the ups and downs of this journey, even while they are embarking on adventures of their own.

My parents, who were never quite sure what I was working on, but continued to support me anyway.

Table of Contents

Signature Page iii

Dedication iv

Table of Contents v

List of Figures vii

List of Tables viii

List of Abbreviations ix

Acknowledgments xi

Vita xiii

Abstract of the Dissertation xiv

Chapter 1: Introduction 1

1.1 Background 1

1.2 Dissertation Overview 19

Chapter 2: Highly conserved *Nmf9* gene is essential for vestibular function 22

2.1 Abstract 22

2.2 Introduction 23

2.3 Results 25

2.4 Discussion 31

2.5 Materials and Methods 37

Chapter 3: Future Directions and Concluding Remarks 73

3.1 Summary 73

3.2 Future Directions 79

3.3 Concluding Remarks 83

Appendix: Protocols.....84

A.1: Protocol for Sodium Hydroxide Extraction of Mouse Tail DNA.....84

A.2: Protocol for RNA Extraction.....85

A.3: Protocol for Quantitative Real-Time PCR of *Nmf9* and Homologs …....86

A.4: Protocol for Creating Stable Tet-on Cell Lines ….....87

A.5: Protocol for Generating CRISPR Mutants in Mice.....88

References 89

List of Figures

Figure 2.1. Positional cloning identifies *Nmf9* 49

Figure 2.2. *Nmf9* expression pattern predicts new sites of function 50

Figure 2.3. *Nmf9* is involved in CNS development 51

Figure 2.4. Mutant animals show age and sex-dependent differences in vestibular dysfunction 52

Figure 2.5. Mutant animals have no detectable auditory dysfunction 53

Figure 2.6. Nmf9 plays a role in fear learning and circadian rhythm 55

Figure 2.7. No obvious impairments are detected for functions of VMH, LS, and PC 56

Figure 2.8. Nmf9 protein is highly conserved in Metazoans 59

Figure 2.9. *Nmf9* orthologs are more highly conserved in related species than paralogs 61

Figure 2.10. Expression of *Nmf9* homologs suggest conservation of function 62

Figure 2.11. Nmf9 interacts with ARF5, a small G protein 66

Figure 2.12. Nmf9 is a cytoplasmic protein 67

Figure 2.13. CRISPR alleles fail to complement founding *nmf9* allele 71

List of Tables

Table 2.1. Circadian phenotypes of *Nmf9* 58

Table 2.2. Species used in evolution conservation analysis 63

Table 2.3. Oligo primers used in experiments 68

Table 2.4. Plasmid constructs 70

Table 2.5. Summary of vestibular test results in CRISPR-generated mutants 72

List of Abbreviations

AMY	Amygdala
ARF	ADP-ribosylation factor
ARL	ARF-Like protein
BBS	Bardet-Biedl Syndrome
BFA	Brefelden A
CAPS	Calcium-dependent Activating Protein for Secretion
CNS	Central nervous system
COPI	Coat Protein I
CRISPR	Clustered Regularly Interspaced Short Palindromic Repeats
ELMOD	ELMO-domain containing 1
ENU	N-ethyl-N-nitrosourea
ER	Endoplasmic Reticulum
GAP	GTPase Activating Protein
GEF	Guanine nucleotide Exchange Factor
GGA	Golgi-localized, Gamma-ear containing, ARF-binding protein
IP	Immunoprecipitation
JAX	The Jackson Laboratory
LAP	Localization and affinity purification
LS	Lateral septum
MCOLN	Mucolipin
mRNA	Messenger ribonucleic acid
NMD	Nonsense mediated decay

PC	Piriform cortex
PCDH	Protocadherin
PCR	Polymerase chain reaction
PFA	Paraformaldehyde
PI4K	Phosphatidyl-inositol-4-kinase
PIP5K	Phosphatidyl-inositol-4-phosphate-5-kinase
PLD	Phospholipase D
qRT-PCR	Quantitative real-time PCR
RACE-PCR	Rapid amplification of cDNA ends PCR
SCN	Suprachiasmatic nucleus
TVC	Tubulo-vesicular cluster
UTR	Untranslated region
VLGR	Very Large G-Protein Coupled Receptor
VMH	Ventral medial hypothalamus
VZ	Ventricular zone
Y2H	Yeast Two-Hybrid

Acknowledgments

The work presented here would not have been possible without the help and support of many scientists both past and present who have been involved in my project either directly or peripherally.

I would like to thank Bruce Hamilton, my thesis adviser, for the lessons he has taught me of both how and what it means to be a scientist. Thank you, as well, for creating the sort of laboratory environment that is particularly friendly for junior scientists to train and grow in, and for allowing me to run with my own project and try new things when I was a first year with a degree in plant biology.

I am grateful to the members of my thesis committee-- Drs. Don Cleveland, Michael Gorman, Yishi Jin, and Binhai Zheng-- for their feedback over the years and for challenging me not only on my research, but on my presentation skills as well. Dr. Gorman, especially, has been both a mentor and a key collaboration on my project. Many of the things I have learned from my committee have already proven to be useful for my future career trajectory.

This project would not have covered the scope it does without the aid of many collaborators, and as I compose my list of individuals to thank I find it difficult to separate out my collaborators from my mentors, since many of them have seved in both capacities to some extent and have taught me so much. This list of individuals include Drs. Amanda Roberts, Elizabeth Keithley, Anita Herman and Wilson Clemens. I would like to also thank the members of the Hamilton Lab – Dr. Wendy Alcaraz, for teaching me how to work with mice and for hand-holding over the years; Dorothy Conception, Drs. Glen Seidner, Lisbeth Flores-Garcia, and Chen-Jei Hong for their continued support and mentorship in many areas outside of my expertise; and Kevin Ross, my fellow

graduate student for his support and enthusiasm. Thank you, everyone.

The content of chapter 2, in part, is being prepared for publication. The author of this dissertation is also the author of this manuscript and the primary researcher. Dr. Bruce Hamilton performed the positional mapping and cloning and identified the mutation. Tiffany Poon performed the northern blot and, in collaboration with Drs. Xiaobo Wang and Elizabeth Keithley, performed and analyzed the inner ear histology. Dr. Michael Gorman performed the circadian behavior tests and assisted with data analysis. The fear conditioning test, acoustic startle test, elevated plus maze and open field test were performed at the Neuroscience Blueprint Behavior Core under the directions of Dr. Amanda Roberson. The material and protocols for my work in fruit flies were provided by Dr. Anita Herman. The material and protocols for my work in zebrafish were provided by Dr. Wilson Clemens. *In situ* hybridization in sea anemone was performed by Drs. Patricia Lee and Mark Martindale. The CRISPR oligomers were designed and synthesized by Kevin Ross and Dr. Bruce Hamilton and injected at the UCSD Transgenic Mouse Core by Ella Kothari and Jun Zhao. The tet-on system vector was kindly provided by members of Dr. Christopher Glass' laboratory.

Vita

2005-2008 Bachelor of Science, University of California, Davis

2008-2014 Doctor of Philosophy, University of California, San Diego

Fellowships

2009-2011 Genetics Training Grant
Univeristy of California, San diego
National Institute of General Medical Sciences T32 GM008666

Publications

Zhang, S., Ross, K.D., Poon, T.P., Gorman, M.R., Wang, X., Keithley, E. M., Hamilton, B. A. 2014. ---------- *Manuscript in Preparation*

Berry, A.M., Mendoza-Herrera, A., Guo, Y., Hayashi, J., Persson,T., Barabote, R., **Zhang, S.**, Pawlowski, K. 2011. New perspectives on nodule nitrogen assimilation in actinorhizal symbioses. **Functional Plant Biology.**

Abstract of the Dissertation

Understanding Locomotor Deficits by Analysis of *Nmf9* Gene

by

Shuxiao Zhang

Doctor of Philosophy in Biomedical Sciences

University of California, San Diego, 2014

Professor Bruce A. Hamilton, Chair

Neuroscience mutagenesis facility (Nmf) 9 is the name of a mouse mutant discovered as part of the Jackson Laboratory NMF N-ethyl-N-nitrosourea (ENU) mutagenesis program in 2002. The *nmf9* mouse mutants were observed to show tremor and signs of vestibular dysfunction, though there were no obvious signs of deafness despite the shared developmental pathways of the vestibular and the auditory system. At the time of the observation, the *nmf9* mutation had not been mapped, and the identity of the gene that is mutated as well as the gene's potential functions were all unknown.

Preliminary data in our laboratory identified *nmf9* as a single point mutation at a splice site, leading to an exon-skipping frame-shift in a novel, low-expressing transcript. The research presented in this dissertation demonstrates that the *Nmf9* transcript is important to both vestibular development in embryos as well as functions in distinct

neurocircuits in the adult brain. Furthermore, *Nmf9* encodes a protein that is conserved throughout Metazoa, and shows some conservation in its functions in the Central Nervous System (CNS) and in mechanosensory structures. Lastly, the work presented here shows the first link between vestibular dysfunction and ADP-Ribosylation Factor (ARF) 5. Though various class I and class III ARFs have been linked to vestibular development via knockdown (KD) of either the ARF itself or other members of its interaction network, this is the first time that a class II ARF has been shown to play a role in this system.

Chapter 1: Introduction

1.1 Background

1.1.1 Challenges in diagnosis and treatment of vestibular dysfunction

Despite the fact that nearly 70 million Americans were affected by vestibular dysfunctions between 2001 and 2004, diagnosis remains difficult (Agrawal et al., 2009). Self-reported symptoms of dizziness and vertigo are vague at best and symptoms can be caused by many conditions unrelated to vestibular dysfunction(Holmes and Padgham, 2011). Vestibular diseases, also known as vestibulopathies, can be divided into five categories: episodic ataxia, benign recurrent vertigo, bilateral vestibulopathy, vertigo migraine, and familial audiovestibular dysfunction (Jen, 2008). Although vestibulopathy is not a disorder with high mortality rates, it can cause imbalance and postural instability, leading to falls. Serious injuries as a result of falls are one of the leading causes of death in elderly individuals, and as the population ages, the cost of vestibulopathy at a societal level is becoming increasingly obvious (Agrawal et al., 2009).

Despite the prevalence of vestibulopathies, their epidemiology and genetic basis are poorly understood, which further hinders diagnosis and treatment. Of the different causes and presentations of vestibular dysfunction, the genetic basis for three of the seven types of episodic ataxia and one type of vestibular migraine have been identified. Mutations in potassium channel *KCNA1,* calcium channel *CACNA1A,* and solute carrier *SLC1A3* are known to cause episodic ataxia*,* while a mutation in progesterone receptor *PGR* has been shown to be associated with one type of vestibular migraine (Jen, 2008).

Many presentations of vestibulopathy have suggestive links to migraine (Lempert and Neuhauser, 2009), though the exact link for comorbidity of these presentations is poorly understood. Zingler et al (Zingler et al., 2009) showed that among patients with vestibulopathies that are characterized by impairment or loss of function in both inner ears, the definitive cause is identified in only 24% of the cases.

Understanding vestibular development and function is important for accurate diagnosis and treatment of vestibular dysfunction. Though many genes and regulatory pathways are shared between the auditory system and the vestibular system during development, there remain many steps in development and function that are unique to the vestibular system that we are only beginning to understand(Kelley, 2006). Given that many of the patients who are diagnosed with vestibulopathies present vestibular dysfunction without obvious auditory symptoms, studying the genes and pathways that diverge between the vestibular and the auditory system, in addition to those that are conserved, could prove to be an important a line of inquiry.

1.1.2 *nmf9* as a novel vestibular mutant

Nmf9 (Neuroscience Mutagenesis Facility 9) is the mutation generated in a large-scale N-ethyl-N-nitrosourea (ENU) mutagenesis screen at the Jackson Laboratory. Jackson Laboratory describes *Nmf9* animals as vestibular mutants with head bobbing and tremor phenotype, but no gross anatomical abnormalities. Preliminary ear sections of the animals performed by the Jackson Laboratory show presence of otoliths, grossly normal semicircular canals, and no obvious hearing deficits. *Nmf9* mutants belonged to one of the groups of mutants whose mutation had yet to be identified, and whose cause of phenotype remains unknown (jaxmice.jax.org).

1.1.3 Additional phenotypes of *nmf9* animals

In addition to the highly penetrant vestibular dysfunction, previous unpublished experiments in our laboratory identified the *nmf9* transcript. Identification of the *Nmf9* transcript early on allowed prediction of additional phenotypes from expression databases. Many of these phenotypes require behavioral screens and would not be obvious under normal housing conditions.

Nmf9 mice show tremor, though they do not show obvious signs of hypomyelination that are found in other tremor mutants such as *shiverer, jimpy,* and *trembler (Popko et al., 1987; Skoff, 1976; Suter et al., 1992; Vela et al., 1998).* In addition, the central nervous system (CNS) of *nmf9* animals appear grossly normal in anatomy and show no obvious signs of spongiform degeneration such as that found in *vibrator* and *wobber (Bird et al., 1971; Weimar et al., 1982)*. The combination of vestibular dysfunction and tremor in *nmf9* mice resembles the phenotype of Mbp^{shi} and *Nmf118.* However, these mutants show defects in hearing and/or vestibular morphology as well as degeneration of the CNS, which are phenotypes not found in *nmf9* animals (see chapter 2).

In addition to tremor, expression data from the Allen Brain Atlas predicts that the function of the amygdala (AMY), the suprachiasmatic nucleus (SCN), the lateral septum (LS), the ventromedial hypothalamus (VMH), and the piriform cortex (PC) may be affected. The AMY is a limbic structure that is considered to be essential to the acquisition of tone-cued fear. Lesions in AMY cause in deficiencies in fear learning when the behavior of the lesioned animals is compared to that of control animals (Agnostaras et al., 1999). In humans, ablation of the AMY has been used to treat violent behavior. Furthermore, there is evidence that it plays an important role in emotional learning and

memory as well (Afifi and Bergman, 2005). The SCN is responsible for the generation of circadian and ultradian rhythms as well as synchronization of these rhythms to environmental light cues (Shigeyoshi et al., 1997). Mice deficient in the expression of SCN-specific genes such as *Clock* and *mPer2* show a slight change in circadian rhythm when they are housed with the appropriate light-dark cycles and a complete absence of circadian rhythm when the light cue is removed (Hotz et al., 1994; Zheng et al., 1999). LS is shown to function in innate anxiety. Lesions of the lateral septum appear to reduce innate anxiety in animal experiments, though different subdivisions of the septum may be either anxiolytic or anxiogenic (Menard and Treit, 1996). Destruction of the LS nuclei in humans tends to lead to behavioral overreaction to most environmental stimuli (Afifi and Bergman, 2005). The VMH is responsible for satiety and metabolism (King 2006). Insulin receptor signaling of subpopulations of neurons in the VMH is important for high-fat diet-induced obesity, and lesions in the VMH induce hyperphagia and obeisity in animals (Yi et al, 2011; King 2006). The PC is part of the primary olfactory cortex and plays a role in olfactory perception and odor discrimination (Stettler and Axel, 2009; Wilson and Stevenson, 2003). Irritative PC lesions in humans cause disagreeable olfactory hallucinations, usually as a prelude to an epileptic fit (Afifi & Bergman, 2005).

1.1.4 Structure and function of the vestibular system

The vestibular system can be roughly divided into central and peripheral components. The peripheral vestibular system is composed of the vestibulocochlear nerve and the five vestibular organs in the inner ear: the utricle, the saccule, and the three semicircular canals (Afifi and Bergman, 2005). In contrast to this, the definition of the central vestibular system in the literature is less clear. The central vestibular system includes the vestibular nuclei and associated pathways in the brain, where signals from

the peripheral vestibular system, the body, and the retina are integrated (Desmond, 2004). There is still considerable controversy as to which neural structures in the brain may be considered a part of the central vestibular system in addition to the vestibular nuclei. It is known that the vestibulocochlear nerve separates once in the brain and the vestibular nerve projects to the vestibular nuclei. The vestibular nuclei output to the cerebellum, the oculomotor nuclei, and the thalamus, though there is also evidence that the vestibular nuclei receive input from the vestibular cortex in the temporal lobe (though the specific region varies). In addition, the central vestibular system has been suggested to be connected to other regions influencing autonomic reflexes of the body such as blood flow and heart rate (Afifi and Bergman, 2005; Tascioglu, 2005). The inferior olive, the cervical and pedal joint receptors, and the hippocampus have all been suggested as part of the central vestibular pathways (Beitz and Anderson, 2000; Desmond, 2004).

The vestibular system detects and processes an organism's sense of position and movement in space. The utricle and saccule are responsible for the sense of position in space and can detect changes in linear acceleration. During movement, the otolithic membrane, a gel-like substance containing small crystals called otoliths, slides over the hair cells, the sensory receptors of the system. This shift of the otolithic membrane bends the hair cells and causes their sensory receptors to fire. The three semicircular canals, extending from the utricle, are set at an angle to each other in order to sense angular acceleration. They work via a mechanism similar to that of the utricle and the saccule. Each semicircular canal has one enlarged region at each end called the ampulla, which contains hair cells whose tips are embedded in a gelatinous structure called the cupula. During rotational movement, the cupula moves with the flow of the endolymph-- the fluid filling the canals. Sensory information from these vestibular organs is then transmitted via Scarpa's ganglia in each ear, which together form the vestibular

nerve. The vestibular nerve and the cochlear nerve form the vestibulocochlear nerve, which projects to the vestibular nuclei in the brain (Afifi and Bergman, 2005; Tascioglu, 2005). The vestibular nuclei, together with the visual system and the oculomotor nucleus, are responsible for vestibulo-ocular reflex and gaze stabilization. The vestibular nuclei, the medial longitudinal fasciculus, the vestibulospinal tracts and reticulospinal tracts are responsible for the vestibulo-cervical reflex and the vestibulo-spinal reflex, which are necessary for upright posture and balance. Finally, the vestibular nuclei also project to the thalamus and cortex, and together they are responsible for the perception of body orientation and personal space (Purves et al., 2008).

1.1.5 Key genes in vestibular development

Many genes important to normal embryonic development play a role in the formation of the vestibular system, which begins around E7.5 with the formation of the otic placode. The otic placode then invaginates to form the otic vesicle around E10.5. Patterning and cell differentiation to form the vestibuloauditory structures in the peripheral system occur around E15.5 (Sumantra et al., 2010), but the central vestibular neuron does not mature until 2-3 weeks after birth, and its input affects the maturation of dopaminergic neurons in the brain (Eugène et al., 2009). Development of the vestibular system utilizes well-known signaling pathways such as *Notch* signaling. As a result of this, the vestibular system has been cited as a model to study temporal and spatial regulation of cell fate and lateral inhibition.

Notch in particular has an important role during early inner ear development. Expression of *Notch* is necessary for the formation of prosensory patches in the otic vesicle for differentiation into sensory epithelia. *Notch* signaling also promotes the expression of *Jagged1* in the inner ear and allows progenitor cells to enter a prosensory

state so that they are competent for differentiation into either hair cells or support cells (Brooker et al., 2006). The *Jagged1* mutation is homozygous lethal due to vascular defects. Heterozygous mutants lack the posterior and sometimes anterior section of the semicircular canals and the remaining vestibular structures appear flattened (Kiernan et al., 2001). *Foxg1-Cre* conditional knockout of *Jagged1* in the inner ear, during the formation of the otic vesicle, results in loss of semicircular canals and small and misshapen utricles and saccules. This suggests that *Jagged1* is essential for the development of the sensory structures in the vestibular system (Kiernan et al., 2006). *Foxg1* by itself is expressed in the otic placode and the inner ear ganglion. Null mutants of *Foxg1* lack horizontal ampulla and have abnormal innervation of the inner ear. Current research suggests that *Foxg1* may operate as part of the *Notch* signaling pathway via *Hes* heterodimers (Pauley et al., 2006).

Notch has another important role during later stages of inner ear development. The differentiation pathway of hair cells is regulated by *Notch and Atoh1. Atoh1* is a transcription factor that promotes differentiation of progenitor cells into hair cells and is thus commonly used as a marker for hair cell progenitors. Although the *Atoh1* null genotype is perinatal lethal, conditional *Pax2-Cre* knock-out of *Atoh1* in the inner ear epithelium results in mice with grossly normal inner ear structures but undifferentiated sensory epithelia (Pan et al., 2011). *Notch* acts as the antagonist to *Atoh1* in this context (Jeon et al., 2011). *Notch* is expressed in progenitor cells which, during the onset of differentiation, express two ligands of *Notch, Delta1* and *Jagged2.* These two ligands promote the differentiation of progenitor cells into support cells (Lanford et al., 1999).

In addition to *Atoh1,* there is evidence that the *Notch* signaling pathway acts in concert with the *Wnt* signaling pathway during inner ear development. When conditional mutants have constitutively active Wnt signaling in the inner ear, the pattern of

expression of *Notch1* as well as *Jag1* is expanded. *Notch* and *Wnt* play a role in defining the size of the otic placode and though there is not sufficient evidence to suggest one directly regulates the other, *Wnt* signaling is capable of up-regulating components of the *Notch* pathway, and *Wnt* signaling is reduced in *Notch1* mutant mice (Jayasena et al., 2008).

There is still much that is unknown about the signaling pathways responsible for regulating development of the inner ear into the vestibular system as opposed to the auditory system, though there is evidence that suggests *Wnt* signaling may play an important role (Kelley, 2006). Constitutively active *Wnt* signaling or over-expression of *Wnt3a* leads to development of vestibular sensory patches in the auditory compartment of the inner ear (Stevens et al., 2003). Another component of *Wnt* signaling*, Dlx5,* appears to be important for patterning of the dorsolateral region of the otic vesicle that would develop into the vestibular compartments. *Dlx5* is required for the formation of semicircular canals. Forced activation of *Wnt* signaling with lithium chloride results in expansion of *Dlx5* expression in the inner ear, while loss of *Wnt1* and *Wnt3a* results in loss of expression of *Dlx5* in the inner ear (Riccomagno et al., 2005).

1.1.6 Conservation of the vestibular system

In addition to understanding the etiology and developing potential treatments for vestibular dysfunction, the vestibular system provides a good model to study the regulation of many key genes involved in embryonic development. The mammalian inner ear is a complex organ and its development requires finely tuned spatial and temporal regulation of signaling pathways such as *Notch,* which is well-known for regulation via lateral inhibition. The *Notch* lateral inhibition/activation pathway is known to play a key role in the fate of neural crest cells and spinal cord development. In the inner ear, this

particular method of signaling regulates the fate of progenitor cells to form the particular pattern of hair-cells and support cells needed.

Notch and many genes involved in inner ear development are highly conserved and predate the evolution of the inner ear. Thus, studying the evolution of these genes in signaling pathways across lineages can provide valuable insight regarding their regulation. Changes in regulation and expression can be estimated by studying the changes in rate of conservation in protein domains across species and lineages. A high rate of conservation at a particular binding site, for instance, would predict protein domains of high functional importance, and a decreased conservation rate at that site in a particular lineage can predict changes in function (Hopitzan et al., 2006; Simon et al., 2002). Comparison across genomes in different lineages can also be used as a method to identify candidate genes for a pathway or structure of interest, such as that of sensory cilia (Avidor-Reiss et al., 2004).

The origin of the vestibular system can be traced back to lineages that predate the evolution of the inner ear, such as mechanosensory organs in fruit flies and the mechanosensory cilia in sea anemone larvae. The mechanosensory bristles of a fruit fly in particular have been suggested to be homologous to the sensory patches in the vertebrate inner ear (Eddison et al., 2000). This conservation has been essential to the discovery of much of what we know of the *Notch* signaling pathway. One component of *Notch* signaling inhibition in mammalian inner ear development that has been conserved in function is *Atoh1. Atoh1* is short for *Atonal* Homolog 1 and, as the name suggests, the mammalian *Atoh1* is homologous to the *Atonal* gene in flies. *Atonal* is essential for the development of the chordotonal organ in fruit flies, which is one of the species' main organs for mechanosensation and balance. Even though *Atonal* does not appear to respond to *Notch* lateral inhibition as the mammalian system does, expression of the

mammalian *Atonal* homolog, *Atoh1,* is sufficient to induce the ectopic growth of chordotonal organ in fruitflies (Ben-Arie et al., 2000). This indicates a high degree of conservation of the *Atoh* gene functions in mechanosensory organ development.

Lampreys represent the most basal vertebrate lineage to have otic placodes, a structure that in mammals develop into the inner ear. In lampreys, the otic placodes develop into a proto-inner ear containing two semircircular canals and an otolith-containing vestibule (Richardson et al., 2010). The lamprey otic placodes, like the otic placodes in mammals, express *Dlx.* This suggests that *Dlx* signaling in placode development has been conserved as far back as the origins of the vertebrate lineage (Neidert et al., 2001).

Zebrafish is the most basal lineage that has an inner ear structure homologous to mammals. The peripheral vestibular system in zebrafish contains both a utricle, a saccule, and three semicircular canals. In addition to the inner ear, zebrafish has another system for sensing movement and vibration in water, called lateral lines, which contain hair cells similar to those found in the inner ear. Zebrafish is an anamniote and the transparency of zebrafish embryos provides additional benefits to the study of inner ear development. Work in zebrafish has identified the conserved roles of *Pax2* and *Pax8* in inner ear development. Even though *Pax2* and *Pax8* are regulated by different factors, deletion of both *Pax2* and *Pax8* is needed for developmental failure of the inner ear while individual deletion results in much milder inner ear defects (Hans et al., 2004). *Atoh1* signaling is also conserved in zebrafish. The zebrafish genome contains two different *Atoh1* genes– *Atoh1a* and *Atoh1b.* Both copies are necessary for hair cell development in zebrafish and both appear to utilize the same signaling pathway as mammals, such as lateral inhibition signaling by *Notch* (Millimaki et al., 2007). The role of *Atoh1* in the development of hair cells both in the lateral line system and in the

zebrafish inner ear corroborates the more ancestral role of *Atonal* in fruit fly mechanosensation and balance (Itoh and Chitnis, 2001).

Despite the similarities that allowed zebrafish to be used as a model for vestibular development and function, there are still key differences that require the use of amniotes such as chick and mice. One of these differences is that in the amniotes, the vestibular structure develops from the dorsal otic vesicle and the semicircular canal ducts are formed from the side pockets of the otic vesicles, whereas in anamniotes they are formed from the tips of projections of those pockets. Though chicks have seven vestibular components instead of five found in mammals, they are one of the most ancestral vertebrate lineages that rely solely on the inner ear for vestibular input, and have long been used to study vestibular development. Studies done in chicks were key to the discovery of *Dlx5/6* signaling via the *Wnt* pathway and *Hmx2/3* signaling in the development of the vestibular structures from the otic vesicles *(Riccomagno et al., 2005).* Though *Wnt* signaling is one of the more ancestral signaling pathways in metazoans, the differentiation between auditory and vestibular hair cell physiology and function is more recent. Thus, the studies in chicks that led to the discovery of *Wnt* signaling in this differentiation suggest at least one additional role *Wnt* has played in the course of mechanosensory development (Stevens et al., 2003).

Vestibular mutants are by far the most well-studied in mice. Mice have a five-compartment peripheral vestibular system and corresponding vestibular nuclei in the brain which are homologous to those found in humans. This conservation, along with the plethora of tools available for genetic manipulation and the established paradigm for using mice to model human diseases, contributed to the relative popularity of the mouse as a model organism in vestibular dysfunction.

1.1.7 Understanding vestibular dysfunction using mouse mutants

Vestibular mutants in mice can be visually identified by characteristic phenotypes such as circling, head nodding, and head tilt. Additionally, batteries of behavioral tests have been established to assess and quantify vestibular dysfunction (Hardisty-Hughes et al., 2010). Many vestibular mutants exist, though nearly all of them show additional phenotypes affecting other systems. The most common non-vestibular phenotype present in these animals is that of auditory impairment.

Many of the mutants that suffer from dysfunction of peripheral vestibular system tend to show additional non-vestibular phenotypes. The most common phenotype in vestibular mutants is partial to complete loss of hearing, most likely due to the shared progenitor cells and regulatory pathways of the vestibular and auditory systems. Many of the genes involved in inner ear development play major roles in other parts of the body as well. As a result, many of the vestibular mutants will show phenotypes unrelated to the vestibuloauditory system (Freyer et al., 2011; Kelley, 2006; Sumantra et al., 2010). A small sampling of these mutants includes the *jerker* mice, which carry a mutation in *Espn.* These animals show circling, degeneration of hair cells, and deafness (Zheng et al., 2010). Another mutant, *ozzy*, shows absence of the vestibulo-ocular reflex and absence of parts of the vestibular system, in addition to deafness and heart defects (Vrijens et al., 2006). *Ozzy* mutants have a missense mutation in *Jag1,* a *Notch* receptor, and illustrate the importance of the *Notch* signaling pathway in the inner ear as well as elsewhere in the body (Kelley, 2006). *Stargazer* is another mutant with additional non-vestibular phenotypes, where a mutation in *Cacng2* results in vacuolization of sensory epithelia in the inner ear as well as epilepsy and cerebellar ataxia (Khan et al., 2004). Inner ear degeneration is also seen in *shaker-1* mice, which carry a mutation in *Myo7A.* Mutation in *Myo7A* in humans causes Usher's syndrome type 1B, which can be

characterized by deafness and retinal degeneration (Gibson et al., 1995). Abnormal inner ear structure, deafness, and kidney defects appear in mice carrying an IAP insertion in the *Eya1* gene. This mutant has been used a model to study branchio-oto-renal (BOR) syndrome (Johnson et al., 1999). A mutation in *ELMOD1,* a GTPase-activating protein (GAP) for ARF-family proteins, results in mice with malformed hair cells and impaired hearing and balance (Johnson et al., 2012).

Much more rare in the literature are mouse mutants that show vestibular phenotypes but normal auditory functions. Mutants of *head-tilt* (*het*) lack otonia and show behaviors characteristic of vestibular dysfunction. *Het* mutants carry a mutation in *Nox3,* and have normal hearing despite the fact that *Nox3* is expressed in both the vestibular and auditory systems (Bánfi et al., 2004; Paffenholz et al., 2004). Vestibular mutants such as the *ci3* rats have normal inner ear morphology and hearing but circle as a result of asymmetrical dopamine distribution in the striatal region of the brain (Lessenich et al., 2001). Similarly, *chakragati* mouse mutants circle as a result of asymmetrical distribution of dopamine receptors (Fitzgerald et al., 1992). It is worth noting that the vestibular mutants that circle as a result of dopamine asymmetry will favor one direction of circling, while the majority of the vestibular mutants do not appear to show a preference and will circle bidirectionally. Lack of directional preference is indicative of peripheral vestibular dysfunction. Of the mutants that show circling with no directional preference, *het* mutants represent a rare example where the vestibular phenotype is divorced from an auditory phenotype. *Nox3* activity is regulated by the ubiquitously expressed small GTPase, *Rac1,* and it is not known what regulates the high expression of *Nox3* in the inner ear (Oxidases, Ueyama, & Leto, 2006). The rarity of *het* phenotype points out the paucity of knowledge regarding what differentiates the hair cells in the vestibular system from those in the auditory system. Though the

development of inner ear structures from otic placodes has been relatively well studied, there remains much to be learned regarding the molecular cues necessary for cell-fate determination of the specialized cells.

1.1.8 ARF protein family and its role in vestibular function

ADP-ribosylation factor (ARF), named for its function as a cofactor in cholera-toxin-catalyzed ribosylation of G protein, is a family of small GTPases known for their function in protein trafficking. ARFs are ubiquitously expressed and distributed throughout the cell. Similar to other small GTPases of the Ras superfamily, all ARFs cycle between an active, GTP-bond form and an inactive, GDP-bond form. The exchange between GTP and GDP-bond forms are facilitated by Guanine nucleotide Exchange Factors (GEFs) and GTPase-Activating Proteins (GAPs). Unlike other Ras-related small G proteins, however, ARFs are inserted in the membranes at their sites of action by their N-termini, which are myristolated, whereas the other small GTPases are inserted by their C-termini. This has led to the hypothesis that effectors of ARF must be positioned close to the membrane surface, in contrast to the other small G proteins. (Donaldson and Jackson, 2011)

Homologs of ARFs have been found in all Eukaryotes that have been studied, from fungi to humans. There is enough conservation between invertebrates and vertebrates that expression of mammalian *ARF1* is sufficient to restore lamellipodium formation in *Drosophila* cells where *ARF79F* (the *ARF1* homolog) has been silenced (Humphreys et al., 2012). The ARF protein family contains three classes of ARFs, which are referred to simply as class I, II, and III. Over 20 ARF-like (ARLs) proteins have been identified based on sequence conservation. Many of the functions of ARLs are currently unknown, though they are hypothesized to have broader functions than ARFs and may

play a role in microtubule functions (Kahn et al., 2005).

Class I ARFs include ARF1, 2 and 3. ARF1 is conserved from yeast to humans and is one of the most well-studied ARF proteins. It is affiliated with Sec7-class GEFs and is known to bind to Coat Protein I (COPI) proteins and Golgi-localized, Gamma-ear containing, ARF-binding proteins (GGAs). Much work has been done to demonstrate the role of ARF1 in *cis*-Golgi transport and transportation between Golgi stacks, where ARF1 recruits clathrin for COPI-coated vesicle budding. ARF1 is also shown to be important in lipid homeostasis at the Golgi by recruiting and stimulating activity of phosphatidyl-inositol-4-kinase (PI4K) (D'Souza-Schorey and Chavrier, 2006).

Class II ARFs are the least well studied and are hypothesized to have arisen more recently compared to the other two classes of ARFs. Unlike class I ARFs, class II ARFs associate with GEFs that are not sensitive to treatments of Brefelden A (BFA) (Duijsings et al., 2009). Its two members, ARF4 and 5, are known to bind to Golgi-Endoplasmic Reticulum (ER) intermediate compartment membranes. They have been suggested to function in *trans*-Golgi trafficking, though decreasing ARF4 and 5 appears to impair retrograde trafficking at the *cis*-Golgi level as well (Kahn et al., 2005; Nakai et al., 2013). Class II ARFs, like other ARFs, can bind and activate phosphatidyl-inositol-4-phosphate-5-kinase (PIP5K) as well as phospholipase D (PLD), suggesting a role in regulation / maintenance of lipid content in Golgi (D'Souza-Schorey and Chavrier, 2006). There is evidence that ARF4 functions with ARF1 in the early secretory pathway and regulates endosome recycling and retrograde transport from Golgi to ER (Nakai et al., 2013). ARF4 has been shown to be part of a complex that is critical for transport of protein to specialized cilium, though the exact mechanism behind the transportation remains unclear. ARF5 appears to pair with ARF1 in retrograde trafficking from tubulo-vesicular cluster (TVC) to ER. GDP-bound ARF4 and 5 can directly bind to Calcium-

dependent Activator Protein for Secretion (CAPS), which suggests a role for class II ARFs in exocytosis of vesicles from nerve terminals (Sadakata et al., 2010), though ARF5 has also been implicated in clathrin-mediated endocytosis. (Moravec et al., 2012)

ARF6 is the sole class III ARF, and the most divergent from the other members of the family by sequence conservation. Unlike the other ARFs, ARF6 does not localize to the Golgi and remains instead at the plasma membrane (Nakai et al., 2013), where it regulates endocytic protein trafficking and plays a role in actin and cell membrane remodeling. As the most well-studied ARF besides ARF1, ARF6 has been shown to associate with GEFS that are insensitive to BFA and mediates endocytosis via clathrin-mediated pathway. ARF6 is also required for endosome recycling via the action of PLD and there is evidence that suggests that ARF6 is involved in cell adhesion and migration (D'Souza-Schorey and Chavrier, 2006; Donaldson and Jackson, 2011).

Various studies of ARF mutants over the years have examined the function of ARFs in whole organisms. Most of the studies that center around ARF mutants are performed in various cell lines or yeast, most likely due to the fact that mutations in ARFs severely affect protein trafficking and often result in lethality as a phenotype. Mutation of ARF1 in yeast results in secretory defects, though mutants of ARF2 are indistinguishable from wildtype. However, mutation of both *ARF1* and *ARF2* is lethal (Stearns et al., 1990). In fruit flies, knockout of *ARF79F*, the homolog of mammalian *ARF1/3*, induced pupal lethality, and mutation in the fly ARF-GEF, *Gartenzwerg,* leads to tracheal defects and is embryonic lethal. *ARF1* is expressed in the inner ear of zebrafish, and knockdown of *ARF1* results in delayed semicircular canal formation in over 90% of the animals at the 48 hour stage, and abnormal semicircular canal morphology at the 72 hour stage. Though these animals show shortened body axis, reduced eye size, and curved tails, no lethality or behavioral phenotype was reported in the paper. Despite the morphological

defects in the inner ear, the induction of otic placode and otolith formation appears grossly normal in these animals (Petko et al., 2009). Unlike class I ARF, class II ARFs do not exist in yeast, the hypothesis being that diversification of ARFs into class II ARFs occured during the Metazoan lineage (Donaldson and Jackson, 2011). No obvious phenotype was reported for the knockout of ARF102F, the homolog of mammalian ARF4/5, in *Drosophila.* (Armbruster and Luschnig, 2012). *ARF5* expression has been found in the notochord of zebrafish at 14-19 somite stage. Though there is a point mutation of ARF5, *sa23226*, in zebrafish, there are no published studies so far on its effects (Thisse et al., 2001). In class III ARFs, mutation of *ARF6* in mice shows perinatal lethality (Donaldson and Jackson, 2011). No other ARF mouse mutant has been documented in the literature, though JAX is in the process of creating a conditional allele of *ARF2* on a *Cre-Sox2* background (jaxmice.jax.org). As a result it is not known whether any of the other ARFs are essential for survival.

In addition to the 2009 paper by Petko et al. (Petko et al., 2009), there are many other instances in the literature where the ARF pathway has been linked to vestibular development and function. ELMO-domain containing 1 (*ELMOD1*) and 2 function as GAPs for ARF family proteins, and mutation of *ELMOD1* has been shown to cause circling behavior and deafness in mice, due to stereocilia degeneration. (Johnson et al., 2012) *Mucolipin* 3 (*MCOLN3*) shares 75% sequence similarity with *MCOLN1* and *MCOLN2.* Mutation of *MCOLN3* results in mice that show hearing loss and vestibular dysfunction. *MCOLN2* is localized to ARF6-regulated pathways and all three MCOLN proteins have been shown to play a role in the vesicular trafficking pathways (Martina et al., 2010). Two genes known to cause Usher's Syndrome are Protocadherin 15 (*PCDH15)* and Very Large G-Protein Coupled Receptor 1 (*VLGR1),* and both proteins have been identified in specific ARF1 positive vesicle pools that are trafficked to the

apical aspect of hair cells in mice. Usher's Syndrome is characterized by deafness, progressive retinitis pigmentosa, and splayed stereocilia in the inner ear of zebrafish and mouse models (Zallocchi et al., 2012).

Other ARF family proteins have been associated with ciliary structures as well. One example is the ARL2 protein, which is essential for the localization of ARL2-binding-protein (ARL2BP). ARL2BP normally localizes to the basal body and the cilium-associated core in photoreceptors, and is important for normal photoreceptor function. Mutation of this gene will cause retinitis pigmentosa (Davidson et al., 2013). Bardet-Biedl Syndrome (BBS) is a ciliopathy characterized by symptoms including but not limited to mental retardation and blindness. It has been linked to eight genes, one of which is *ARL6* (Kahn et al., 2005). Indeed, the importance of ARF family proteins to cilia appears to be highly conserved, as the protein ARL-5b is essential to the repair of mechanosensory cilia in sea anemones, which represent a much more ancestral lineage (Watson et al., 2007).

1.2 Dissertation Overview

The genetic mutation in Neuroscience Mutagenesis Facility 9 (*nmf9*) mice disrupts a gene that encodes a novel neuronal protein. The mutants display impaired vestibular function in addition to tremor and head-tossing, but the mechanisms that cause these traits are unknown. Unpublished work in the laboratory has shown that the animals have normal hearing and that the inner ear, the vestibular nuclei, and the associated regions are grossly normal in anatomy. The expression of *Nmf9* is enriched in specific areas in the brain, though it is unclear whether the functions of those brain regions are uniformly affected in the mutants or how they contribute to the vestibular phenotype. The aims of the work presented in this dissertation are to understand the function of the gene with a three-pronged approach. The first aim focuses on the mutation itself and include assays for behavioral traits that are known to require the anatomical systems that express the *Nmf9* transcript. The second aim focuses on conservation and uses data available from the transcripts of *Nmf9* homologs to predict the role of Nmf9 protein in the cell by identifying potential domains of functional importance. The third aim focuses on the Nmf9 protein, and utilizes proteomic tools with the predicted protein domains to place Nmf9 in interaction pathways. This aim approaches the function of *Nmf9* by connecting the study of the single point mutation we have identified in the gene, to the protein that it encodes, to the multitude of phenotypes we have observed in the animals.

Aim1: Determine functional deficits in *nmf9*

Although preliminary data showed a scattered pattern of *Nmf9* expression throughout the adult brain, certain regions of the brain, most notably the amygdaloid and

suprachiasmatic nuclei but also the lateral septum, the ventromedial nuclei of the hypothalamus and the piriform cortex, show much higher levels of expression. I hypothesized that the neuronal systems that are enriched in *Nmf9* will show functional abnormality in the mutants. I assayed the animals for signs of abnormal circadian cycle, abnormal weight gain, elevated innate anxiety, impaired cued fear conditioning, and impaired olfaction using established methods. By testing the function of these circuits this aim seeks to identify the cellular context in which *Nmf9* plays an important role. I also hypothesized that *Nmf9* may play additional roles during development in addition to what preliminary data has predicted in adult animals. To test this hypothesis, I performed *in situ* hybridization across a series of developmental time points in order to identify additional times and sites of expression.

Aim2: Comparison of evolutionary constraints across different animal lineages

Based on preliminary data, some invertebrate orthologs include a C-terminal Ras Association (RA) domain while mammalian homologs do not. Basal vertebrates have one paralog of each kind. Urochodates, a sister group to vertebrates, completely lack the gene. I hypothesized that the evolutionary constraints in Nmf9 protein are unequal across known functional domains and unequal between different animal lineages. I calculated sliding window evolutionary rates along the imputed Nmf9 protein sequence for each animal lineage to test for divergence of function and to predict possible universal and lineage-specific functional domains. In addition I have performed *in situ* hybridization to examine the localization of the homologs in other organisms in order to correlate potential conservation of expression patterns with conservation of domains. This aim seeks to provide a framework for contextual and biochemical features important to Nmf9 by quantifying lineage specific rates of evolution along the protein and by testing

whether conservation changes along the protein are correlated with changes in expression pattern and, potentially, regulation and function.

Aim3: Determine the physical interaction network of Nmf9

Preliminary data indicates *Nmf9* expression is neuron-specific in vertebrates and the protein contains domains that are known to mediate protein-protein interactions. I hypothesized that Nmf9 directly interacts with specific proteins in the neuronal signaling pathways which are responsible for cellular deficits in the mutant, which lead to the observed vestibular phenotype and tremor. I tested this hypothesis by using co-immunoprecipitation and mass spectrometry to identify the main interaction partner of Nmf9 and used conservation information from aim 2 to create protein fragments to test the specificity of the interactions. Co-localization studies were used to test the likely relevance of potential interaction partners. The focus of this aim is to gain insight into how Nmf9 functions by defining its molecular context and placing it within known protein interaction networks.

Chapter 2 contains results of aim 1-3 and forms the basis for a manuscript that is currently in preparation for publication.

Chapter 3 contains future directions regarding the exploration of *Nmf9* function within a protein network, as well as its role in neurodevelopment outside of the vestibular system.

Chapter 2: Highly conserved *Nmf9* gene is essential for vestibular function

2.1 Abstract

A large fraction of protein-coding genes identified by genome sequences remain without functional annotation or biochemical context. Here we describe a novel protein-coding gene required for neurological function in mice. Positional cloning of *nmf9* identified a novel transcript that encodes two ankyrin repeats, one fibronectin type III domain, and three highly conserved domains that do not match any known motifs. *Nmf9* is expressed in the inner ear and brain of both embryonic and adult animals. Null mutants have vestibular dysfunction, tremor, impaired fear learning, and circadian abnormalities. The animals have normal hearing, with no gross histological defects in the inner ear and brain. Affinity purification and mass spectrometry identified ADP-ribosylation factor (ARF) 5 as a key interaction partner. These results suggests that the Nmf9 protein may be a new component required for vesicular trafficking in neurons.

2.2 Introduction

Many protein-coding genes identified by genome sequences remain of unknown function despite conservation across considerable evolutionary distance. This group may include genes whose functions affect fitness but not overt phenotypes in experimental settings, genes that affect overt but less well-studied phenotypes, and/or genes that have been difficult to study due to unusual molecular properties, such as low level expression or poor physical annotation in genomes of well-studied organisms. While high-throughput analyses can provide hints, direct study is often required to enumerate functions of novel genes, particularly those whose properties make their study more challenging. Forward genetics offers one entry point into functional studies by highlighting those genes whose alterations produce measurable effects (Beutler et al., 2007; Justice et al., 1999). A key challenge in de-orphanizing novel genes is to integrate their function with known cellular activities.

ADP-ribosylation factors (ARFs) are a highly conserved subfamily of small GTPases that regulate intracellular trafficking and organelle structure in plants, animals, and fungi (D'Souza-Schorey and Chavrier, 2006). ARFs are generally divided into 3 classes: Class I (ARF1-3) regulate ER to Golgi and Golgi to endosome vesicles. Class III (ARF6) regulates endocytic vesicles (from plasma membrane to endosome). Class II (ARF4,5) is the least well studied, but current literature suggests they regulate early Golgi and trans-Golgi vesicles. ARF proteins interact with specific GTP exchange factors (GEFs) and GTPase activating proteins (GEFs). ARF5 will interact with BRAG2, GGA3 GBF1, PSCD4 and potentially adaptin complex, and MINT1-3 (Kahn et al., 2005; Moravec et al., 2012; Takatsu et al., 2002). Mutations in class I and class III ARF-mediated pathways cause vestibular dysfunction (Johnson et al., 2012; Martina et al.,

2010) but the details of the relationship between the mutation and the phenotype remain unclear. No data to date has tied class 2 ARFs to neurological systems nor have there been studies on the effects of ARF5 mutation on an organism.

The *nmf9* mutation was isolated in an N-ethyl-N-nitrosourea (ENU) screen and recognized by its vestibular phenotype and tremor at the Neuroscience Mutagenesis Facility of the Jackson laboratory. Here, we mapped *nmf9* to a novel transcript expressed at low levels. Although it is highly conserved among animals, it remained poorly annotated in most genomes and without demonstrated function in any. Its expression pattern in mouse brain and sensory structures suggested a requirement for *nmf9* in several discrete neurological functions and we confirmed a subset of these predictions with behavioral tests. In addition to canonical ankyrin and fibronectin repeats, evolutionary constraint among >90 homologs identified novel domains of functional importance. We used affinity purification and mass spectroscopy to identify the small GTPase Arf5 as one binding partner of the mouse Nmf9 protein. Homologs in other Metazoan and Holozoan species contain additional domains suggesting interactions with other small GTPases of the Ras superfamily.

2.3 Results

2.3.1 Positional cloning of *nmf9* reveals novel gene expressed at low abundance

Mutants homozygous for the recessive *nmf9* mutation show vestibular phenotypes such as head nodding and circling in addition to tremor. Recombination mapping of the vestibular phenotype in ~1000 F2 progeny among crosses of B6-nmf9 to four different mapping strains (332 AKR/J; 245 BALB/cJ, including192 from JAX; 371 C3H; 119 DBA/2J) placed the *nmf9* mutation in a 1.3 Mb interval (Chr11: 88,240,426-89,538,743 in GRCm38/mm10 assembly) (Fig. 2.1 A), with no evidence of strain-dependent modifiers. All canonical and EST exons in mutant and littermate controls for that region were sequenced using the Sanger method, and a single point mutation was identified (Fig. 2.1 B). A G-to-A transition at a splice donor U1 binding site causes skipping of a frame-shifting exon, potentially targeting the mutant transcript for nonsense mediated decay (NMD) (Fig. 2.1 D-E). *Nmf9* is a low abundance transcript in control animal, expressing at a ratio of, on average, 2.25E10-8 molecule *Nmf9* to 1 molecule of *GAPDH* in qRT-PCR, with even lower abundance in mutants (Fig. 2.1 E-F), further suggesting NMD. The mutation is located in the transcript annotated as *Ankfn1* (Fig. 2.1 C). Northern blot data with probes covering the entire transcript indicate that *Nmf9* transcript contains both the transcript annotated as *Ankfn1* as well as the transcript annotated as *4932411E22Rik* (E22), and that there exists one main isoform of *Nmf9* transcript though RACE-PCR indicates that there may be multiple 5' ends possible (Fig. 2.1 F, RACE-PCR data not shown). Additional alleles of *nmf9* generated using the Clustered Regularly Interspaced Short Palindromic Repeats (CRISPR)/Cas system (Wang et al., 2013) failed to complement the founding *nmf9* allele in assays of vestibular function (Fig. 2.13, Table 2.5). qRT-PCR data with sets of primers designed for putative

UTRs for either *Ankfn1* or *E22* or *Nmf9* as a joint transcript that bridges the intron gap provides further proof that *Nmf9* exists as one transcript, and that neither *Ankfn1* nor *E22* are transcribed separately as independent transcripts (Fig. 2.3 C).

2.3.2 Nmf9 expression pattern predicts function in multiple neurological systems

Nmf9 is expressed as early as E14.5 in the inner ear, nasal epithelium, and ventricular zone as well as the spinal cord. (Fig. 2.3 A-B.) In embryos, *Nmf9* is expressed in the same population of cells in the vestibular system that express *Atoh1* (Fig. 2.2 A), a known marker for inner ear hair-cell progenitors (Kelley, 2006), which corresponds with the observed phenotype of vestibular dysfunction. Expression in the brain persists in adults in the ventral medial hypothalamus (VMH), amygdala (AMY), lateral septum (LS), the piriform cortex (PC), and the suprachiasmatic nucleus (SCN), each with known neurological correlates, suggesting additional functional impairment. Probes that correspond to predicted genes *Ankfn1* and *E22* showed the same pattern, further confirming unity of the transcription unit (Fig. 2.2 B).

2.3.3 Vestibular dysfunction in *nmf9* mice is sexually dimorphic and progressive

Mutant mice often display signs of vestibular dysfunction such as circling, nodding, and head-tilt. This is quantified with the landing test and the forced swim test (Fig. 2.4 A-B). In the landing test, animals were scored by investigators blinded to the genotypes for trunk curling and attempts to rotate while suspended by their tails, and mutant animals show a significant increase in frequency of these phenotypes when compared to wild type littermates. In the forced swim test, wildtype littermates can easily swim with their snout above water for over one minute, whereas mutants often display a tumbling behavior underwater and must be rescued after a few seconds to prevent

drowning. Despite this, mutant animals have inner ear structures that are grossly normal (Fig. 2.5 A) and no obvious hearing impairment was detected by either acoustic startle response (Fig. 2.5 B) or preliminary acoustic brainstem response test (10 mutants and 2 controls, data not shown). All mutant phenotypes showed incomplete penetrance for all assays, with females more frequently and more severely affected than males. The same assays performed on mice as they age at 21 days, two months, and 6 months indicate that the effected status for specific measures increased with age (Fig. 2.4 C-F).

2.3.4 Fear-conditioned learning and circadian behaviors are impaired in mutants

Nmf9 expression is enriched in VMH, AMY, LS, PC, and SCN (Fig 2.2 B), each of which is known to be essential for certain neurological functions and behaviors. AMY is known to be essential to the circuit for fear learning, which appears to be impaired in *nmf9* animals. Mutants are assayed for learned-fear related phenotypes with contextual and cued fear conditioning and show a significant decrease in freezing behavior compared to wildtype littermates, post training. Decreased fear response was sex biased, with strong defects in female mutants but only nominal trend in males (Fig. 2.6 A). SCN is known to be essential for circadian behavior. The more severely affected *nmf9* mice show signs of arrhythmia when compared to wildtype littermates (Fig. 2.6 B). Mutants also show an increase in onset error, a slight shortening of period, and their hyperactive phenotype did not significantly affect activity counts in either LD or DD housing conditions (Fig. 2.6 C, Table 2.1).

VMH plays a role in satiety and lipid metabolism. Mutant animals show a slight but significant decrease in weight compared to wildtype littermates, which is detectable at two and six months (Fig. 2.7 A) but no significant difference in the amount of food consumed (Fig. 2.7 F). Function of LS, which is involved in innate anxiety, was tested

with elevated plus maze and open field test. No significant difference was detected with elevated plus test (Fig. 2.7 D). In open field test, mutants show a significant increase in time spent in center of field, which could indicate a functional lesion in LS. However, the number of line crosses in field is also significantly higher for mutants compared to wildtypes, which suggests that the hyperactive and circling phenotypes may compromise any interpretation of the result (Fig. 2.7 E). Marble-burying test, which is less affected by activity, was used as a follow-up assay, and no significant difference was detected between wildtype and mutant animals (Fig. 2.7 C). Finally, PC is a known part of the olfaction pathway, and though it shows enrichment of *Nmf9* expression, no significant dysfunction was detected in the mutants when the animals were tested with buried food finding test (Fig. 2.7 B) and odor habituation / dishabituation test (Fig. 2.7 G).

2.3.5 *Nmf9* encodes highly a conserved protein with diverged architecture in vertebrates

Homologs of *Nmf9,* built off of annotated genomes of model organisms, are found in all Metazoan lineages except the Urochordate, and a possible event of horizontal gene transfer which resulted in a homolog of *Nmf9* in a species of fungi (Fig. 2.8 A). The homologs fall in poorly annotated regions in most genome assemblies. Analysis of evolutionary constraint using Datamonkey (Pond et al., 2005) across 14 species spaced across evolutionary time confirms the conservation of known ankyrin repeats and fibronectin domain, but also predicts three additional regions of unknown biological function under even higher constraint (Fig. 2.8 B). Of these three regions, domain 2 is the most highly conserved region in the entire protein, with the glycine residues in the GLYGYLK sequence the most highly conserved (Fig. 2.8 C). Substitution of alanine for glycine at this position is sufficient to induce vestibular dysfunction in trans-

heterozygous animals carrying the G612A mutation over the founding JAX allele (Table 2.5). However, no known protein motifs were found in this region in analysis with Motif Scan (http://myhits.isb-sib.ch/cgi-bin/motif_scan), Scansite 2.0 Scan Motif (scansite.mit.edu), Scan Prosite (prosite.expasy.org), InterProScan 4 (http://www.ebi.ac.uk/Tools/pfa/iprscan/), Pfam (pfam.xfam.org), or SMART 6 (smart.embl.de), nor were there predictions of either sulfination, glycosylation, or phosphorylation sites in scans with YinOYang (www.cbs.dtu.dk/services/YinOYang) or The Sulfinator (web.expasy.org/sulfinator).

Vertebrate homologs can be broadly divided into ancestral and derived groups based on their patterns of conservation (Fig. 2.9 A). Mammals carry the derived homolog while the more ancestral lineages such as *C. elegans* and *D. melanogaster* carry the ancestral homolog. Some clades such as the Osteichthyes, the amphibians, and the birds, carry both homologs, suggesting a gene duplication event early in the vertebrate evolution, followed by differentiation and neofunctionalization of one of the copies, before the ancestral homolog is lost in the mammalian lineage. Though domain 2 is the most highly conserved in both ancestral and derived homologs, there is a detectable difference in the conservation signature between the two versions in a detailed analysis containing 113 species (Fig. 2.8 D, Fig. 2.9 B, Table 2.2). In *D. rerio* the peak of expression for the derived homolog appears to differ from the ancestral (Fig. 2.10 B), though both versions, like the homolog in *D. melanogaster* and *N vectensis,* are expressed during developmental stages (Fig. 2.10 A).

2.3.6 Nmf9 is a cytoplasmic protein that interacts with ARF5

Nmf9 protein is endogenously expressed in P19 teratoma cells at low levels. Nm9 protein fused to the Localization and Affinity Purification (LAP) tag at the N-

terminus shows diffuse expression throughout the cytoplasm that does not co-localize with small cytoplasmic vesicles such as endosomes (Fig. 2.12 A) or lysosomes (data not shown). Immunoprecipitation of LAP-Nmf9 fusion protein using anti-GFP antibody has resulted in a novel band in the pulldown lane that mass-spectrometry identified as ARF5 (Fig. 2.11 A-B). LAP-Nmf9 fusion protein does not noticeably co-localize with ARF5 (Fig. 2.12 B) within a cell.

2.4 Discussion

2.4.1 De-orphanizing genes of unknown function requires a multi-level approach

With the advancement of both mutagenesis and sequencing technology, it has become increasingly easy to target and mutagenize genes of interest as well as create and identify novel mutations in genes of unknown function. In cases where there is no literature available, it is still both possible and important to combine tools of molecular biology with information available in databases in order to uncover the function of a novel gene. We describe here the use of combinatorial approaches to study the function of *Nmf9* when there is no background literature readily available for this gene of interest. Starting with the *nmf9* mutant, we identified the point mutation in *Nmf9* using positional cloning. Time and location of gene expression were assayed with ISH to predict genetic function, since none was known. The expression data also predicted additional phenotypes at the behavioral level, confirming that *Nmf9* is pleiotropic. Sequence information at the genetic level identified other homologs both annotated and not, and the additional information was analyzed for patterns of evolutionary constraint to predict functional domains at the protein level. The collective data at the behavioral, genetic and evolution levels was necessary to formulate hypotheses regarding Nmf9 protein function, which is unknown, and allow these hypotheses to be tested with protein interactions experiments.

2.4.2 *Nmf9* affects functions of separate and distinct regions of CNS

Pleiotropic genes with expression in distinct and seemingly unrelated regions are not uncommon. One example of this is that recent studies in circadian biology have shown that there are very few “circadian genes” that are purely circadian. *Rev-Erb α*, for

instance, is a circadian gene that also regulates adipogenesis, while *EGFR* is known to be important for regulation of cell proliferation (Fontaine et al., 2003; Preitner et al., 2002; Zhang and Kay, 2010). Other examples can be found in the vestibular field itself (Kelley, 2006; Sumantra et al., 2010). *Sox2* has a broad expression pattern and is important in many stages of CNS development, in addition to being essential for inner ear development (Kiernan et al., 2005). *Atoh1* is essential to the formation of granule neurons in the cerebellum as well as the development of inner ear hair cells (Bermingham, 1999; Pan et al., 2011).

Nmf9 likewise shows a complex expression pattern in the vestibular system, the olfactory system, and the regions of the brain responsible for satiety and metabolism, innate anxiety, fear-learning, and circadian rhythm (King, 2006; Menard and Treit, 1996; Nicolas et al., 2006; Stettler and Axel, 2009; Zhang and Kay, 2010). The functions of all these systems have been assayed and the mutants show vestibular, circadian, and learned-fear phenotypes. The mutant phenotypes are not fully penetrant and tend to vary more than wildtype phenotypes, which suggests that *Nmf9* is important but not essential to these pathways, and that loss of function mutation reduces the robustness of those neurocircuits. Following this interpretation, it is likely that the functions of AMY, LS, and PC were not disrupted enough for a phenotype to be detected, which could reflect either how essential *Nmf9* is to that system or how tolerant the system is to perturbation. Alternatively *Nmf9* could play a role in phenotype buffering, and loss of function would therefore impair homeostasis. There is no gene that has an expression pattern that matches well with that of *Nmf9* (Allen Brain Atlas), suggesting that *Nmf9* may be involved in different genetic pathways at each site of expression. There is no obvious loss of cell types in any of the nuclei that express *Nmf9*, indicating that it is not essential for cell identity / proliferation of those regions.

We have shown that *Nmf9* is expressed in the inner ear, but not in the vestibular nuclei. *Nmf9* expression is specific to the vestibular organs in the inner ear, indicating that the main vestibular defect is based in the peripheral vestibular system and not the central vestibular system. We have found that the mutant vestibular phenotype is progressive, but the morphology of the *nmf9* inner ear is grossly normal in adult mice (2-3 months in age) and shows no obvious signs of degeneration. This is in contrast with animals carrying a mutation in proteins important for hair cell structure, such as *jerker* or *shaker*, where inner ear degeneration can start as early as post-natal day 11 (Gibson et al., 1995; Zheng et al., 2010). It is also in contrast with animals where the signaling to key developmental pathways is impaired, such as *Sox2* and *Atoh1,* where the mutants show loss of one or more parts of the inner ear (Kiernan et al., 2005; Pan et al., 2011). Therefore, any defect in *nmf9* mutants is likely to occur on a fine scale, such as presence of ectopic hair cells or dentritic defect in the vestibular neurons, which also suggests a possible mechanism for defects in learned fear seen in *nmf9*. When GIT1, an ARF-GAP protein, is knocked out in mice, the animals show impaired fear learning and defects in dendritic spine formation in the hippocampus (Donaldson and Jackson, 2011). *Nmf9,* however, is not expressed in the hippocampus, which suggests that it affects learned fear predominantly through the amygdala.

Our data shows that *Nmf9* plays a role in circadian function, though the protein is cytoplasmic and does not contain any of the known motifs associated with the core transcription-translation oscillation (TTO) loop. We have shown that the main interaction partner of Nmf9 is ARF5, though there is currently no evidence that ARFs play a role in SCN. However, since *Nmf9* is expressed specifically in CNS and is enriched in SCN, it is most likely that *Nmf9* only affects the function of SCN and not other peripheral clocks.

2.4.3 The function of *Nmf9* predates evolution of the inner ear

Nmf9 is conserved throughout the Metazoans, predating the evolution of the inner ear and the *Notch* pathway, both of which are absent in *M. brevicollis (King et al., 2008)*. It is conserved at least as far back as the *Ankryin* gene, which arose at the start of the Metazoans (Cai and Zhang, 2006), indicating that *Nmf9* is likely to have high functional importance. It is consistently expressed at low levels in fruit fly, zebrafish, and mouse, with its expression level peaking during late embryogenesis / early development, suggesting expression regulation is conserved to some degree. Both homologs of *Nmf9* are expressed in the inner ear in zebrafish, and *CG6954*, the fly homolog, is enriched in the CNS, suggesting conservation of function. Additionally, the derived paralog in zebrafish shows a more specific expression pattern than the ancestral paralog, which, given the specificity of expression of the mouse ortholog and the more ubiquitious expression in flies, suggest evolution towards a higher degree of specialization of gene function and the process of neofunctionalization.

The interaction between Nmf9 protein and ARF is likely to represent an evolving but ancestral relationship as opposed to one that is newly evolved. Ancestral homologs of Nmf9 in more basal lineages include additional domains that predict roles for Nmf9 in small GTPase signaling network, such as the RA domain in basal metazoans and the CRIB domain in choanoflagellates. Although these domains are absent in the mammalian homologs, their presence suggest that the interaction between Nmf9 protein and small GTPases predates the gene duplication and divergent evolution of homologs that occurred during the earlier stages of vertebrate evolution. Domain 2, which appears to be important for this interaction, is the most highly conserved domain in both ancestral and derived homologs of this protein, suggesting that the particular interaction with ARF is of high functional importance that may date back to the existence of Nmf9 itself.

2.4.4 Nmf9 is an ARF5 interacting protein

The interaction of ARF5 with Nmf9 protein provides the first link between class II ARFs and vestibular function. Though all ARFs share certain functional similarities, notably in their roles in intracellular trafficking, each ARF is under tight spacial control and works in series or pairs as part of the larger small G protein signaling network (Donaldson and Jackson, 2011). Literature has just started to explore possible links between ARF proteins and vestibular dysfunction, with a focus on class I and class III ARFs. Mutation of the Arf-GAP *Elmod1*, which has been shown to act in class I and class III ARFs, produces deafness and vestibular dysfunction in mice (Johnson et al., 2012). Another part of the class III ARF pathway is effected in mutations of *Mcoln3*, an intracellular Ca2+ channel implicated in an Arf6 endosomal pathway. Mutation of *Mcoln3* results in deafness and vestibular dysfunction in mouse mutants (Martina et al., 2010). For class I ARFs, ARF1 has been shown to be essential to the formation of semicircular canals in zebrafish and is hypothesized to form a complex with NCS1 and PI4K beta (Petko et al., 2009). In contrast, class II ARFS (ARF4 and 5) are thought to be the youngest ARF lineage and are the least well studied. ARF5 is thought to play a role in Golgi transport (D'Souza-Schorey and Chavrier, 2006). The examples of class I and class III ARFs suggest possibilities within actin cytoskeleton assembly within hair cells or signaling defects at the synapse. Certainly there is precedence that a defect in synaptic transmission, such as the *asteroid* mutant, could result in vestibular dysfunction while preserving the normal morphology of hair cells and associated neurons (Obholzer et al., 2008). Potential defects in synaptic transmission also offer an attractive explanation for the dysfunctions affecting multiple distinct regions of the *nmf9* brain. The fact that *nmf9* mutants show vestibular dysfunction but no obvious hearing deficits would suggest that

either ARF5-Nmf9 can be linked peripherally to the *Wnt* signaling pathway, which differentiates vestibular from auditory cells in the inner ear, or that there is a still more elusive pathway of differentiation between the two systems that requires a functional ARF5-Nmf9 interaction.

2.5 Materials and Methods

Genetic Mapping

C57BL/6J–*nmf9* mice were obtained from the Neuroscience Mutagenesis Facility (NMF) and AKR/J, BALB/cJ, C3H/HeJ and DBA/2J from production colonies at the Jackson Laboratory. Markers for genetic mapping were chosen from the Massachusetts Institute of Technology Mouse Genetics and Physical Mapping project (www.borad.mit.edu/cgi-bin/mouse/index). New markers were also typed on a smaller C57BL/6J–*nur12* x BALB/cJ cross performed at NMF. B6-*nmf9* mutant line was maintained on C57BL/6J stocks and genotyped by sequencing PCR products of the mutated region; primers are given in Table 2.3.

Generation of alternative alleles with CRISPR

Alternative alleles of *nmf9* were generated using CRISPR technology as described by Wang et al (Wang et al., 2013). Briefly, *Cas-9* sequence was amplified from plasmid pX330-U6-Chimeric_BB-CBh-hSpCas9 (Addgene #42230) and sgRNA was synthesized as single strand templates (Ultramers, IDT). Both *Cas-9* and sgRNA were amplified via PCR (see Supplemental material for oligomers), transcribed with the mMessage mMachine T7 Ultra Kit (AM1345, Life Technologies), and purified with MEGAclear Kit (AM1908, Life Technologies). Cocktails containing *Cas-9* mRNA, sgRNA, and synthesized repair oligomers (Ultramers, IDT) in embryo-qualified water were injected into the cytoplasm of one cell embryos harvested from C57BL6 (Harlan) mice at the UCSD Transgenic Mouse and Gene Targeting Core.

Cell Culture, Transfection, and Immunofluorescence

P19 cells were maintained in Dulbecco's Modified Eagle Medium containing 10%

FBS and 1% antibiotic:antimycotic. Stable cell lines containing the tet-on system were selected with 0.4ug/mL G418 sulfate (Corning) and hygromycin (Life Technologies). For transfection, P19 cells were seeded into 6 well plates and grown until they reached around 80% confluency. The cells were then transfected with Lipofectamine 2000 (Life Technologies) at a plasmid concentration of 5ug per 12uL Lipofectamine reagent per well. (See Supplemental Table 2.4 for a list of constructs). For expression over 24 hours, cells were washed once with PBS and cultured in Dulbecco's Modified Eagle Medium containing 10% FBS and 1% antibiotic:antimycotic. Selecting reagents were added depending on experiment. Cells for fluorescence microscopy were seeded on poly-D-lysine coated coverslips and transfected overnight. Cells were washed 1x with PBS after 24 hours, fixed with 4% paraformaldehyde in PBS at room temperature for 10 minutes, washed again with PBX, and permeabilized with 0.2% triton-X in PBS for 10 minutes at room temperature. The cells were then blocked with 5% normal donkey serum (Jackson ImmunoResearch) in 0.2% triton-x PBS for 5 minutes then incubated with rabbit anti-EEA1 (Pierce Antibodies, 1:400) in blocking solution at room temperature for 1 hour. After washing 3x with blocking solution samples were incubated with goat anti-rabbit Alexa594 antibody (Invitrogen A11037, 1:1000) at room temperature for 1 hour, then washed 3x in blocking solution and 2x in PBS. Samples were stained with 5ug/mL DAPI at room temperature for 10 minutes and washed 2x in PBS before mounting with Vectashield mounting medium (Vector Lab) and examined under Nikon Eclipse E800.

Northern Blot, qPCR

Northern blots were performed as described in Alcaraz et al (Alcaraz et al., 2006). Briefly, whole brains were dissected from adult animals and RNA extracted using Trizol (Life Technologies), as per reagent protocol. Oligo(dT) cellulose type 7 (Amersham

Biosciences) was used to select mRNA. Around 8.5ug of polyA selected RNA was loaded per lane on a denaturing formaldehyde gel and the content transferred to Hybond-N+ membrane (Thermo Fisher), UV crosslinked, and hybridized overnight with probes synthesized from fragmented 1992.3/.6-pTrcHis and 1992.8/.9-pTrcHis plasmid and random-labeled with P32. Blots were exposed to Phosphor Screen (Molecular Dyamics) for 5 days and imaged with Typhoon Trio Variable Mode Imager.

All quantitative RT-PCR was performed with SybrGreen assay using Biorad Real-Time PCR system on the Bio-Rad CFX96 instrument as described in Concepcion et al (Concepcion et al., 2009). Each sample was measured in triplicate and all samples being compared were run on the same plate. Expression was normalized to *GAPDH* and / or *PitpA* in mice, *GAPDH* and *RP49* in fruitflies, *EF1A* and *SDHA* in zebrafish. (See Table 2.3 for primers.)

In Situ Hybridization

In situ hybridization of mouse tissue was performed as described in (Alcaraz et al., 2006). Briefly, dissected embryos were fixed in formalin, adult mouse brain in 4% PFA. Samples were cryoprotected in 30% sucrose and sectioned at 20um. Fifteen minute treatment with boiling sodium citrate was used for antigen retrieval and slides were treated with acetic anhydride in triethanolamine prior to hybridization. Hybridization was done with 1:25 dilution with *Nmf9* probe and 1:100 *Atoh1* probe. *Nmf9* probe was synthesized from PCR products amplified across the entire *Nmf9* transcript and *Atoh1* probe was synthesized from PCR product of *Atoh1* plasmid clone (see Table 2.3 for primers, Table 2.4 for clone). All were dioxigenin-labeled and the slides hybridized at 65C overnight. Samples were blocked with 5% normal donkey serum (Jackson ImmunoResearch) in PBSTX (0.2% triton-x in PBS) for 1 hour. Samples were incubated

with anti-digoxigenin-AP fab fragments (Roche 11 093 274 910) at 1:2000 overnight at 4C for development. Whole mount *in situ* in zebrafish was performed as described in Clemens et al (Clements et al., 2011). Chromosome 12 homolog was synthesized by linearizing pGEM T vector plasmid containing the insert with NcoI (New England Biolabs) and transcribed with SP6 RNA polymerase (Promega) for anti-sense probe. It is linearized with SpeI (NEB) and transcribed with T7 RNA polymerase (Life Technologies) for the sense probe. Chromosome 24 homolog in pBluescript was linearized with AflIII (NEB) and transcribed with T3 (Life Technologies) for the anti-sense probe, NotI (NEB) and T7 for the sense probe. Samples were fixed in 4% PFA in PBS. Proteinase K was used for antigen retrieval at 10ug/mL for 1 hour at 37C. Hybridization was with 1:20 diluted probes at 65C for 48 hours. Samples were blocked with 2% normal donkey serum, 2mg/mL BSA (NEB) in PBTx and incubated with 1:5000 anti-dig-AP fab fragments overnight at 4C.

Whole mount *in situ* in fruitfly was performed as described by Patterson et al (Patterson et al., 2013). Briefly, embryos and stored in methanol were re-hydrated step-wise in PBST and proteinase K was used for antigen retrieval. Probes were synthesized by linearizing *CG6954* clone with XhoI for antisense, and EcoRI for sense probe. Embryos were hybridized at 55C overnight with 1:20 diluted probes. Samples were blocked with 1:10 Western Blocking Reagent (Roche) in PBTwx (0.1% Tween 20 and 0.1% Triton-X in PBS) and incubated with 1:1000 anti-dig-AP fab fragments for 2 hours at 4C.

Whole mount *in situ* of *N. vectensis* was performed as described by Marlow et al. (Marlow et al., 2012).

Behavioral Assays

All behavioral tests were performed on mice between 2 to 6 months of age, with wildtype littermates of mutants as control, and scored by investigators blinded to the animal's genotype.

Vestibular function. For forced swim test animals were individually placed in a 4L beaker filled with with 3L 25C water and the swim time measured as the length of time an animal was able to keep its snout above water (Paffenholz et al. 2004). For landing test animals were individually lifted by their tails. Normal animals will extend their head and forelimbs toward the ground, exhibiting landing behavior, whereas mutant animals tend to curl their trunk sideways or ventrally and occasionally trying to rotate (Lessenich et al. 2001). The presence of the curling / rotation behavior was scored. For nodding, tremor, circling, and hyperactivity, each animal was placed in a fresh cage and observed for one minute and scored for presence of each phenotype.

Auditory function. The startle response was performed using San Diego Instruments startle chambers (SR-Lab; San Diego, California) by the Behavioral Core at the Scripps Research Institute (TSRI). The chambers consisted of nonrestrictive Plexiglas cylinders 5 cm in diameter resting on a Plexiglas platform in a ventilated chamber. High-frequency speakers mounted 33 cm above the cylinders produced all acoustic stimuli, which were controlled by SR-LAB software. Piezoelectric accelerometers mounted under the cylinders transduced movements of the animal, which were digitized and stored by an interface and computer assembly. Startle pulses started at 70 dB, 40ms in duration, and increased to 120 dB in 5 dB increments and then ramped back down, interspersed by no stimulus trials. The background noise level was at 70dB. Acoustic brainstem response was performed as described by Keithley et al (Keithley et al., 1999).

Learned fear. Fear conditioning was performed by the Behavioral Core at TSRI and took place in Freeze Monitor chambers (Med Associates) stationed in sound-proof boxes. The Plexiglas conditioning chambers (26 x 26 x 17 cm) had speakers and lights mounted on two opposite walls and were installed with a shockable grid floor. On day 1, mice were placed in the conditioning chamber for five minutes to habituate them. On day 2, the mice were exposed to the context and conditioned stimulus (30 seconds, 3000 Hz, 80 dB sound) in association with foot shock (0.70 mA, 2 second, scrambled current). The animals received 2 shock exposures, in the last 2 seconds of a 30 second tone exposure during a 5.5 minute session. On day 3, contextual conditioning in animals was measured in a 5 minute test in the training chamber. On day 4, cued conditioning was measured in a novel context, where the chamber previously used was disguised (new opaque plastic rounded compartment replacing old clear square compartment, new opaque plastic floor replacing metal grid, novel odor with a drop of orange extract under floor). The animals were allowed to habituate for 3 minutes before exposure to the conditioned stimulus (tone) for 3 minutes. Freezing behavior was measured in all sessions by a validated computer-controlled recording of photocell beam interruptions (Contarino et al., 2002).

Circadian function. Mutant and wildtype littermates of either sex, between three-five months of age, were individually housed with food and water *ad libitum.* Activity records were plotted as actograms and analyzed using ClockLab (Actimetrics, Evanston, IL). Unless otherwise noted, all calculations were performed across an interval of approximately 14 days. The period estimates were analyzed with the activity onset predicted by Clocklab (Actimetrics), after manually checking and adjusting when necessary. Power and tau in LD 12:12 and DD were calculated using the batch analysis. Onset tau and onset error the onset of the period of daily activity in DD were

calculated using the adjusted activity onset data. The percentage of activity during daytime was calculated as the number of counts in an eight hour interval that began two hours after the start of the light cycle, normalized to the total activity count per day. Analysis of duration of activity in LD was calculated from the average activity profile as the difference between activity onset and offset, where activity onset was designated as the first three successive bins where the activity count is above average daily activity and the activity offset is designated as the last three successive bins above average daily activity, with the data binned to 30 minute intervals. The average activity profile was calculated by averaging the activity profile of each animal across the fourteen day interval, and the average daily activity was calculated by averaging the activity from the profile. The average Daytime activity was the amount of activity in during an eight hour interval, beginning two hours after the start of the photophase. The percentage of daytime activity was the daytime activity normalized to total average daily activity (Gorman, 2006).

Innate anxiety. Elevated plus-maze test and open field test were performed at the Behavioral Core at TSRI. The plus maze apparatus had four arms (5 X 30 cm) at right angles to each other and was elevated 30 cm from the floor. The two closed arms had 16 cm high walls. The two open arms had a 0.5 cm lip and no walls. Animals were placed in the center of maze and allowed free access to all arms for 5 minutes and their behaviors were recorded with mounted camera The open field apparatus was a square plexiglas (50 x 50 cm) open field surrounded by 22cm walls. The field was divided into 16 squares (12 outer and 4 inner) of equal areas. Animals were placed in the center of the field and recorded for 10 to 60 minute with mounted camera. The marble burying test (De Boer and Koolhaas, 2003; Nicolas et al., 2006) was performed by placing individual animals in a standard mouse cage containing bedding that was 5 cm in depth, with 20

small marbles arranged in 4 evenly spaced rows of 5 on top of the bedding material. After 30 min mice were removed and the number of marbles buried (at least 2/3 covered by bedding) was counted.

Olfaction. Buried food finding test (Crawley, 2008; Yang and Crawley, 2009) was performed on individually housed mice. The animals received one piece of Froot Loops (Kellog's, the same colored cereal was used for all animals) cereal per day with *ad libitum* access to water and normal chow starting 3 days before testing. Fourteen hours (overnight) before testing animals were deprived of food while water remained *ad libitum*. During the test, individual animals were placed into clean cages containing 2cm of bedding, in the corner opposite of the corner where a piece of cereal was hidden. The time for the animal to locate and hold the cereal in both of its paws was recorded with a stop watch. Odor habituation / dishabituation test (Le Pichon et al., 2008; Yang and Crawley, 2009) was performed by placing individual animals in a clean cage and allowing 30 minutes for habituation. Non-social odors were presented before social odors. For non-social odors a cotton-tipped applicator dipped in either de-ionized water or 1:100 dilution of almond or vanilla extract (McCormick &Co) was presented. For social odors each applicator used to swab the inside of a cage housing a single non-littermate animal for three days was presented. The length of time each animal spent investigating the tip applicator was recorded with two minutes given per applicator trial. The same odor was presented in three consecutive trials, with the same order of odor presentation for all animals.

Satiety and metabolism. Animals were weighed at 21 days, 2 months, and 6 months of age. For food consumption test, at the evening of the start of the week food amount sufficient for the week is provided to the animals *ad libitum*. The mass of the food is weighed each subsequent evening at the same time and monitored for spillage

(Crawley, 1999).

Protein Pulldown and Western Blotting

To establish stable cell lines, P19 cells were transiently transfected with pTet-On plasmid (PT3072-5 ClonTech) and selected for resistant single cell colonies. These cells were then transfected with pTRE2hyg plasmid (PT3521-5 ClonTech) containing either LAP tag or LAP-tagged Nmf9 protein sequence (see Supplemental Table 2.4) and double selected for single cell colonies containing both pTet-On and pTR2hyg with G418 (see section under cell culture).

Tet-on cells are induced with 20ug/mL doxycyclin for 24 hours and lysed with CellyticM buffer (Sigma). IP is with 1:1 mix of mouse anti-GFP (MACF 19C8 and MACF 19F7 from Monoclonal Antibody Core Facility at Memorial Sloan-Kettering Cancer Center) at 3ug/mL and 3.5ug/mL respectively. The band specific to Nmf9 in the final eluate was visualized with SilverQuest Staining Kit (Life Technologies) and identified via mass spectroscopy by Biomolecular / Proteomics Mass Spectrometry Facility at UCSD. After removing common artifacts, only peptides whose known or predicted protein weight approximated the observed molecular weight were considered further.

ARF5, ARF6, and Nmf9 fragments were cloned into pET-28C vector (EMD Millipore) for polyhisidine tag and expressed in BL31de3 cells with IPTG induction. His-tagged protein was purified using HisPur Ni-NTA Resin (Thermo Scientific) according to the “Purification of Polyhistidine Containing Recombinant Proteins” protocol from Life Technologies. Resin containing purified his-tagged proteins was incubated in cell binding buffer with S35 labeled Nmf9 fragments and control or ARF5, ARF6, ARF5 locked-form mutants synthesized using TnT T7 Quick Coupled Translation / Transcription System (Promega).

For western blot, eluted proteins were separated on 12% SDS-PAGE, transferred to nitrocellulose membrane, and blocked with Blok solution (Millipore). Primary antibodies used for detection was 1:500 rabbit anti-ARF from Santa Cruz (H-50 sc9603), with 1:2000 goat anti-rabbit heavy-chain specific HRP antibody from My Biosource (MBS674739) as secondary. Protein bands were visualized using Pierce ECL Western Blotting Substrate (Thermo Scientific).

For S35-labeled interactions, eluated proteins were separated on 12% SDS-PAGE and the gel fixed with methanol fixing solution. The gel was dried on a gel drying frame (ISC Bioexpress) between cellophane (Bio-Rad) at room temperature and visualized with Phosphor Screen (Molecular Dyamics) with overnight exposure.

Conservation Analysis and Motif Scans

Protein sequences homologous to mouse Nmf9 were retrieved through NCBI tblastn, UCSC Genome Browser, Ensembl, Origins of Multicellularity Project and JGI. Identified fragments were used to search the full length sequences in surrounding genomic sequences where available (see Supplemental Table 2.2). For homologs inferred purely through genomic sequences, GENSCAN program was used to predict open reading frames (Burge and Karlint, 1998). All database searches were performed before February 2013. For the full-length protein analysis, the best annotated sequence of each evolutionary branch was used. For the high resolution analysis, sequences with more than 50% gaps in that domain were excluded. Predicted cDNA sequences were translated using ExPASy Translate (Artimo et al., 2012) and aligned using MUSCLE (Edgar, 2004) and the result of the amino acid alignment was used to manually correct the nucleic acid alignment. Conservation rates were calculated with Datamonkey (Kosakovsky Pond et al., 2010; Pond and Frost, 2010) using codon data type and

universal genetic code with neighbor joining tree. Motif search was performed with Motif Scan (Pagni et al., 2007), Scansite 2.0 Scan Motif (Obenauer, 2003), Scan Prosite (Sigrist et al., 2013), InterProScan 4 (Quevillon et al., 2005), Pfam (Finn et al., 2010), and SMART 6 (Letunic et al., 2009). Protein modification scan was performed using The Sulfinator (Monigatti et al., 2002) for sulfination and YinOYang (Gupta and Brunak, 2002) for glycosylation and phosphorylation.

Histology

Ear canals from adult and mutant mice were dissected and fixed in 4% PFA in PBS overnight and decalcified in EDTA. Paraffin sections of inner ear were performed as described in Wang et al (Wang et al., 2009).

Data Analysis

Statistical analysis of data presented was performed with programs available from the Vassar Stats public web interface (Fisher's Exact Test, Log-Linear Analysis, ANOVA, Tukey's Test) (Vassar Stats: website for statistical computation, vassarstats.net) and / or with statistical package in R version 3.0.1 (2013-05-16) (ANOVA, Tukey's Test). Fisher's Exact Test and Log-Linear Analysis were used to analyze frequency-based data and two-way ANOVA for quantitative normally distributed data. Bar graphs of summary data were plotted as mean values with standard error of measure shown for the behavioral tests, and standard deviation for all others. Raw circadian data was collected and analyzed using Clocklab software (Actimetrics) and the individual data points plotted along with box-and-whisker plot using R. All other graphs were plotted with LibreOffice Calc.

The content of chapter 2, in part, is being prepared for publication. The author of this dissertation is also the author of this manuscript and the primary researcher. Dr. Bruce Hamilton performed the positional mapping and cloning and identified the mutation. Tiffany Poon performed the northern blot and, in collaboration with Drs. Xiaobo Wang and Elizabeth Keithley, performed and analyzed the inner ear histology. Dr. Michael Gorman performed the circadian behavior tests and assisted with data analysis. The fear conditioning test, acoustic startle test, elevated plus maze and open field test were performed at the Neuroscience Blueprint Behavior Core under the directions of Dr. Amanda Roberson. The material and protocols for my work in fruit flies were provided by Dr. Anita Herman. The material and protocols for my work in zebrafish were provided by Dr. Wilson Clemens. *In situ* hybridization in sea anemone was performed by Drs. Patricia Lee and Mark Martindale. The CRISPR oligomers were designed and synthesized by Kevin Ross and Dr. Bruce Hamilton and injected at the UCSD Transgenic Mouse Core by Ella Kothari and Jun Zhao. The tet-on system vector was kindly provided by members of Dr. Christopher Glass' laboratory.

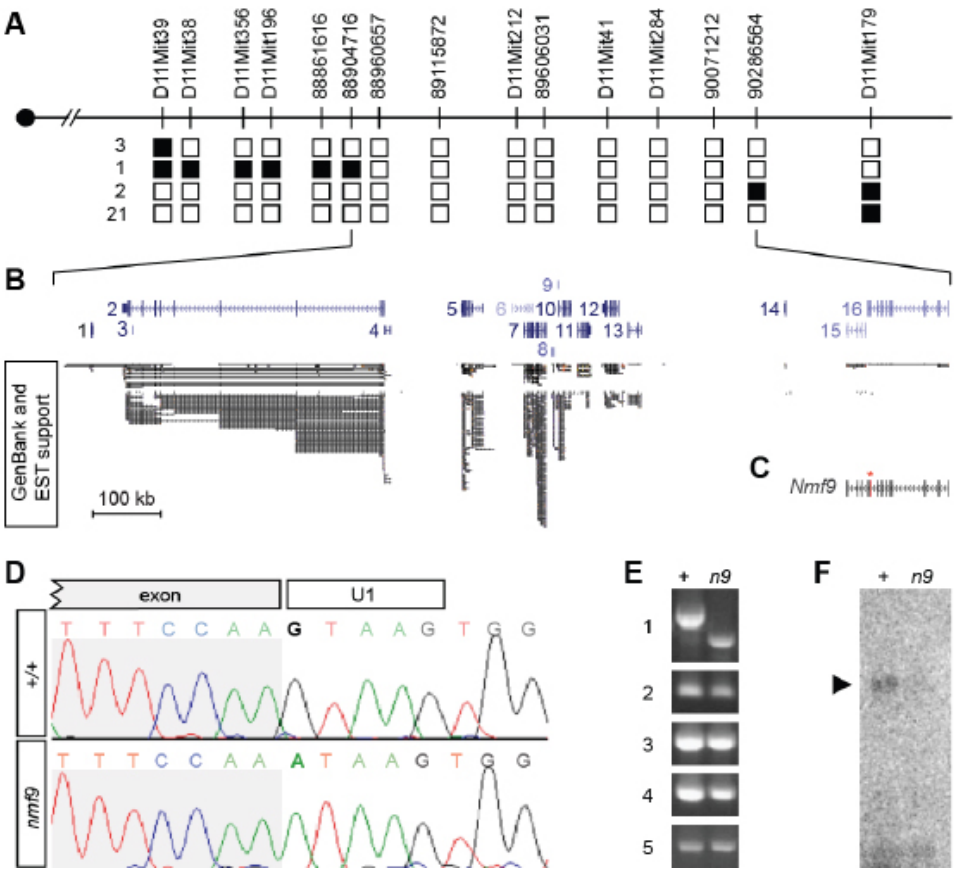

Figure 2.1. Positional cloning identifies *Nmf9.* (A) Recombination mapping places the *nmf9* mutation in a 1.3 Mb interval on Chr. 11. (B) Aligned UCSC Genome Browser window, shows known and predicted genes in the *nmf9* interval. Extent of EST support indicates poor sampling of putative genes *4932411E22* and *Ankfn1*. (C) RT-PCR and exon-PCR sequencing reveals a single mutation (red asterisk) in a *Nmf9* transcript that includes both *E22* and *Ankfn1*. (D) Sanger sequencing across the exon-intron junction shows a G-to-A transition in the essential GU splice donor adjacent to a frame-shifting exon. (E) RT-PCR from priming sites in adjacent exons shows skipping of the exon with the mutated site (panel 1) but not other exons in the same transcript. (F) Northern blot shows reduced level of *Nmf9* transcript in *nmf9* mutant (*n9*) compared to control (+) littermate brain RNA., RACE products.

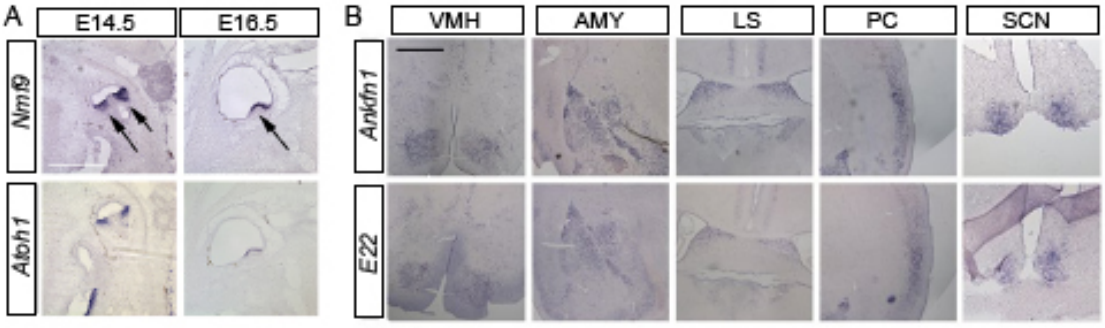

Figure 2.2. *Nmf9* expression pattern predicts new sites of function. (A) *In situ hybridization* of adjacent sections in E14.5 and E16.5 embryos show *Nmf9* and *Atoh1,* a marker of hair cell progenitors, are expressed in the same population of cells (indicated with arrows). Scale bar = 500 microns. (B) *ISH* of adjacent sections in adult brain show *Ankfn1* and *E22* are expressed in identical regions in adult brain not directly linked with vestibular function.

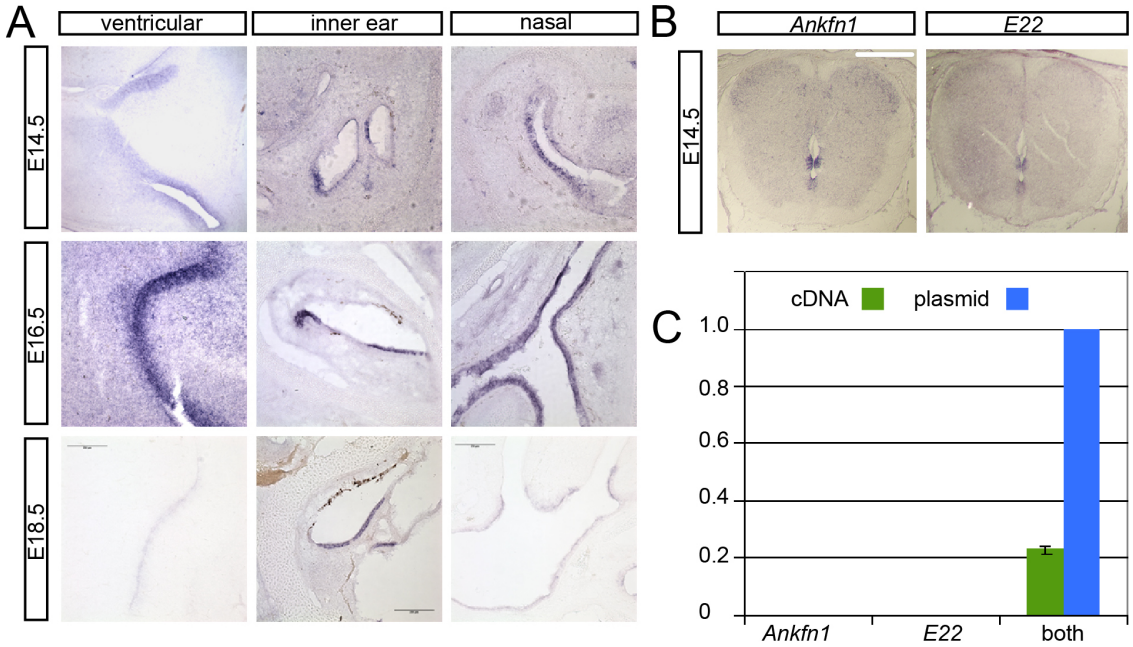

Figure 2.3. *Nmf9* is involved in CNS development. (A) *Nmf9* expression can be detected as early as E14.5 with *in situ* in ventricular zones, inner ear, and nasal epithelium. Expression appears increased at E16.5 and decreased by E18.5. (B) *Nmf9* is expressed in a sub-population of cells around the central canal in E14.5 spinal cord. Scale bar = 500 microns. (C) Neither *Ankfn1* nor *E22* are detected as separate transcripts. *Nmf9* expression is only detected as one transcript containing both.

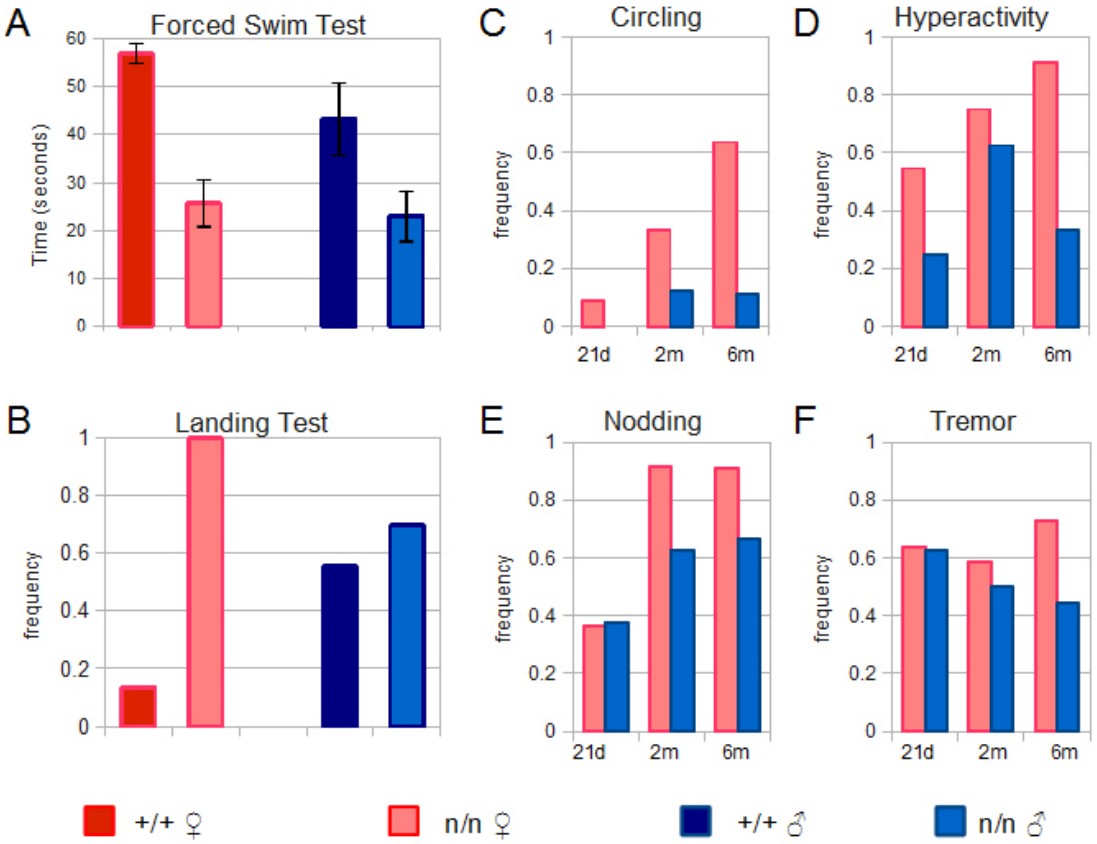

Figure 2.4. Mutant animals show age and sex-dependent differences in vestibular dysfunction. Mutant animals show significant vestibular dysfunction when compared to wildtype litter mates. Female mutant animals show higher penetrance for vestibular phenotype as measured by forced swim test (A) and landing test (B) than males mutants. Error bars =SEM. N = 14 wildtype females, 11 mutant females, 8 wildtype males, 9 mutant males. P-value <0.0001 between genotype, 0.02 between sex for forced swim test; two-way ANOVA. P-value = 0.0234 between genotype, 0.0146 between sex for landing test, Fisher's Exact Test. Animals show age-dependent progression in circling (C), hyperactivity (D), and nodding (E), but not tremor (F), when scored at 21 days, 2 months, and 6 month. N= 11 females, 8 males at 21 days, 12 females, 8 males at two months, 11 females, 9 males at 6 months. P-value = 0.02 for circling, 0.03 for hyperactivity for sexual dimorphism. P-value= 0.04 for nodding, 0.01 for circling, 0.004 for hyperactivity for age-dependent progression. Log-linear analysis for 3-way contingency table (chi-square).

Figure 2.5. Mutant animals have no detectable auditory dysfunction. (A) *nmf9* mutants have ampulla, saccule, Scarpa's ganglion, utricle, and semi-circular canals that are grossly normal in morphology. (B) No significant differences are detected in hearing of adult animals between 2 to 6 months in age. N= 12 wildtype females, 12 wildtype males, 13 mutant females, 7 mutant males. Error bar = SEM. ANOVA.

A

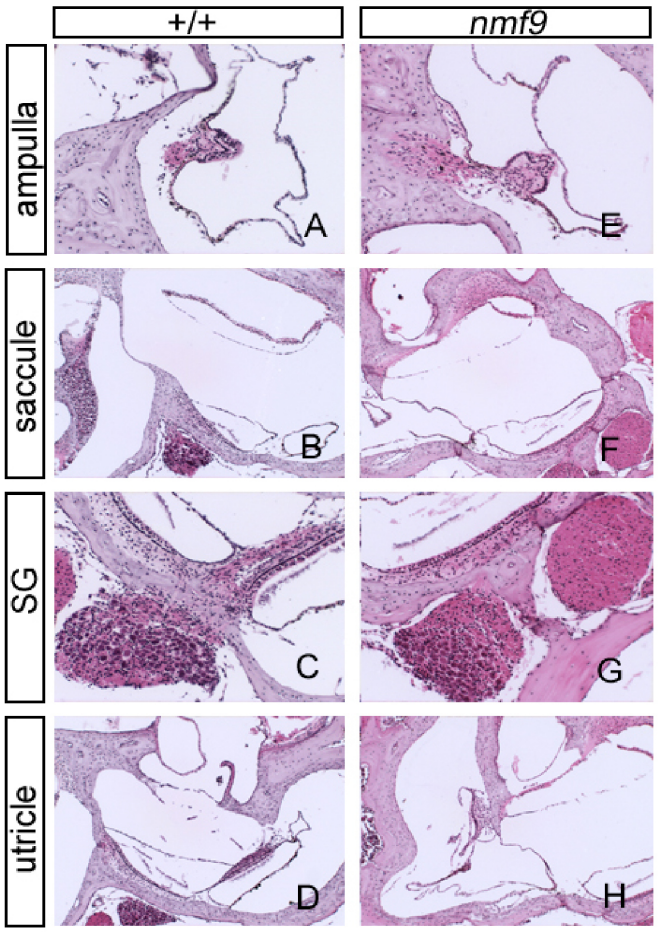
+/+
nmf9
ampulla
saccule
SG
utricle
A
E
B
F
C
G
D
H

B

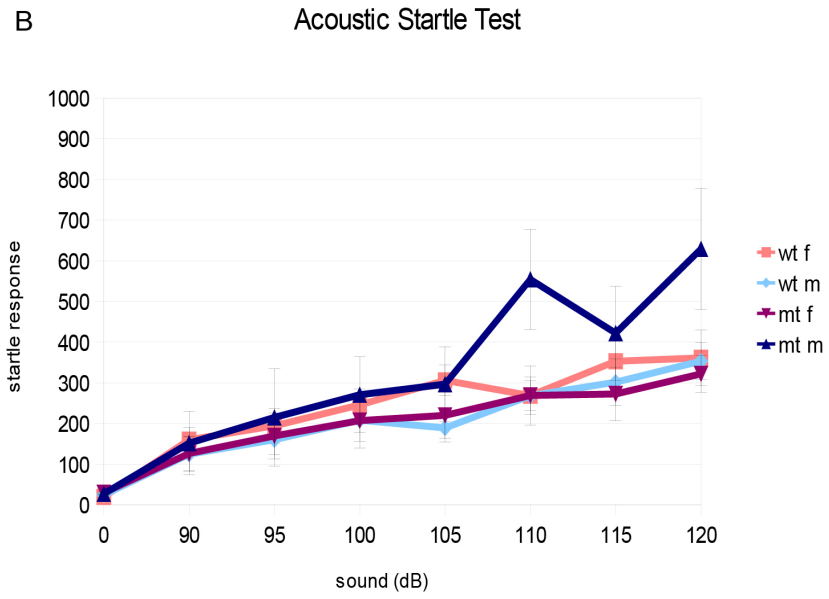
Acoustic Startle Test
startle response
1000
900
800
700
600
500
400
300
200
100
0
0
90
95
100
105
110
115
120
sound (dB)
wt f
wt m
mt f
mt m

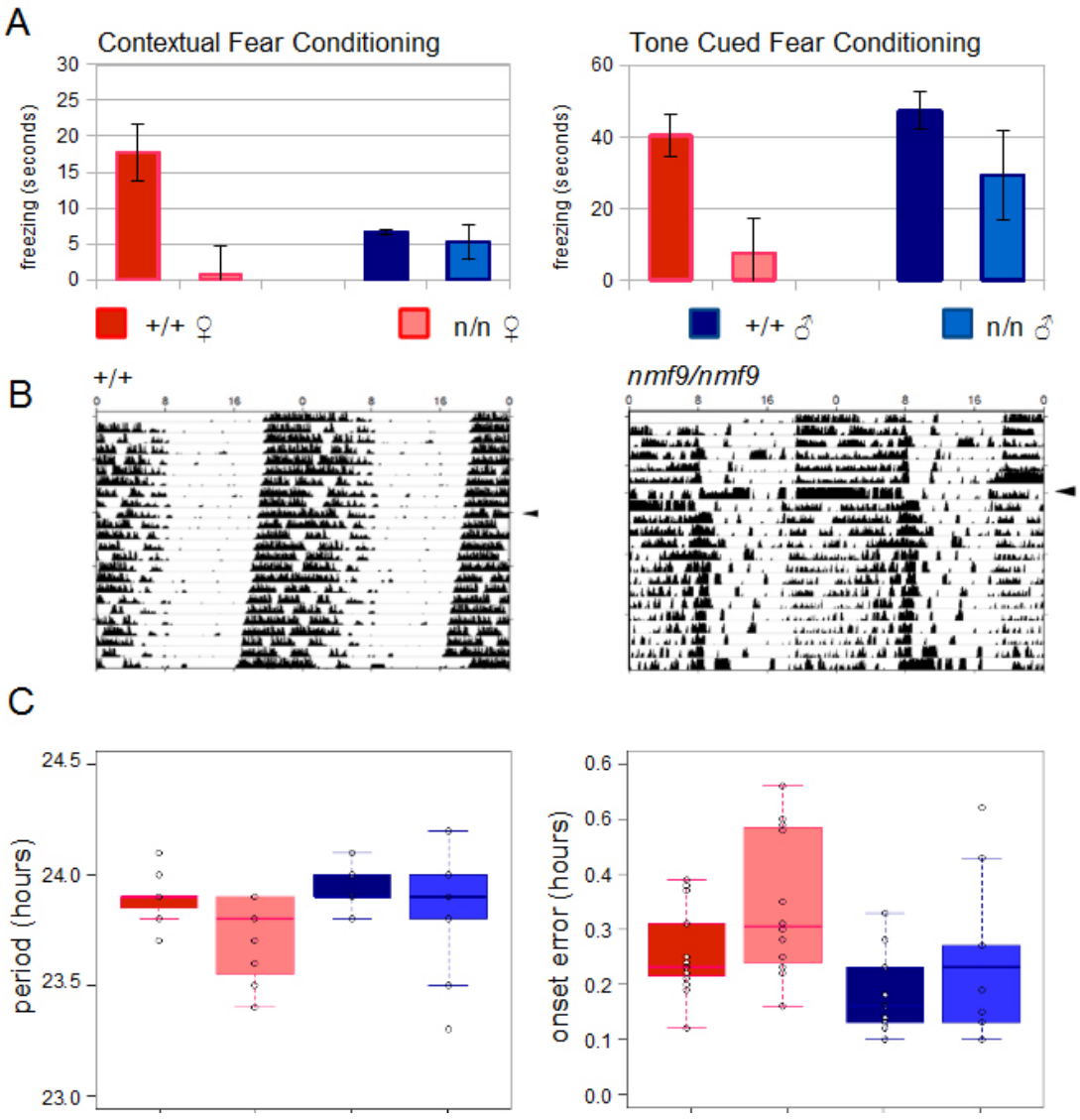

Figure 2.6. *Nmf9* plays a role in fear learning and circadian rhythm. (A) Mutant animals show decreased freezing behavior in both tone cued and contextual fear conditioning. N=14 for wildtype female, 8 mutant female, 11 wildtype male, 8 mutant male. P-value = 0.0018 between genotype for contexual conditioning, 0.002 for tone-cued conditioning, analyzed with two-way ANOVA. Difference between sex N.S. (B) Double-plotted actograms of running-wheel counts of mutant and wildtype from the same litter housed in 12 hour LD cycle and DD cycle show that mutants with decreased robustness in circadian rhythm. Transfer to DD cycle indicated with arrowhead. (C) Based on wheel running data, mutants show slight decrease in period length (P=0.03)and an increase in period onset error (P=0.04) when housed in DD. N= 14 wildtype females, 12 mutant females, 9 wildtype males, 10 mutant males; all data are analyzed using two-way ANOVA.

Figure 2.7. No obvious impairments are detected for functions of VMH, LS, and PC. (A) Mutants weigh less than wildtype littermates at 2 months, and 6 months. P-value = N.S. at 21 days, 0.0002 between genotype, <0.0001 between sex at 2 months, 0.03 between genotype, <0.0001 between sex at 6 months. N= 13 wildtype females, 11 mutant females, 13 wildtype males, 8 mutant males at 21 days, 15 wildtype females, 12 mutant females, 16 wildtype males, 8 mutant males at 2 months, 13 wildtype females, 12 mutant females, 8 wildtype males, 9 mutant males at 6 months. (B) No significant difference is detected between mutant and wildtype in Marble Burying Test or (C) Buried Food Finding Test, N= 10 wildtype females, 9 mutant females, 8 wildtype males, 9 mutant males. Two-way ANOVA is used for all analyses.(D) No significant differences in behavior are detected between wildtype and mutant littermates for Elevated Plus Maze. N= 14 wildtype females, 8 mutant females, 11 wildtype males, 8 mutant males. (E) Mutant animals show increased time spent in center in Open Field Test and increased number of line crosses. P-value = 0.02 for time in center, <0.0001 for line crosses between genotypes. P-value = 0.0004 between sex for line crosses. N= 14 wildtype females, 8 mutant females, 11 wildtype males, 8 mutant males. (F) There is no significant difference between wildtype and mutant littermates in amount of food consumed or in Odor Habituation / Dishabituation Test (E). N= 10 wildtype females, 9 mutant females, 8 wildtype males, 9 mutant males. Two-way ANOVA is used for all analyses.

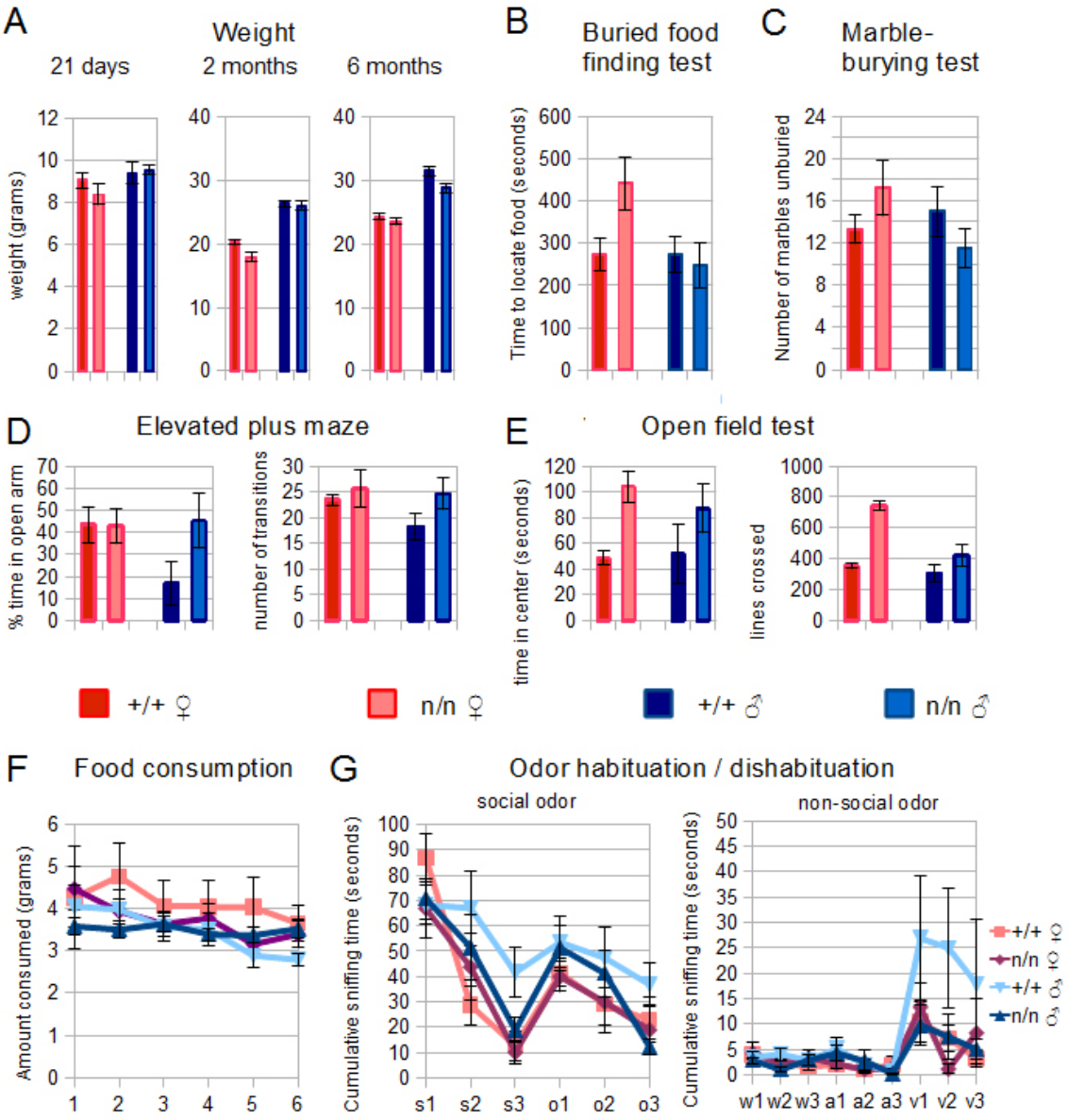
A
Weight
21 days
2 months
6 months
weight (grams)
B
Buried food finding test
Time to locate food (seconds)
C
Marble-burying test
Number of marbles unburied
D
Elevated plus maze
% time in open arm
number of transitions
E
Open field test
time in center (seconds)
lines crossed
+/+ ♀
n/n ♀
+/+ ♂
n/n ♂
F
Food consumption
Amount consumed (grams)
G
Odor habituation / dishabituation
social odor
non-social odor
Cumulative sniffing time (seconds)
s1 s2 s3 o1 o2 o3
w1 w2 w3 a1 a2 a3 v1 v2 v3
+/+ ♀
n/n ♀
+/+ ♂
n/n ♂

Table 2.1. Circadian phenotype of *Nmf9.* Animals are housed in 12:12 LD cycles for a minimum of 7 days prior to transition to DD. Tau, power, and onset are calculated as average over ~14 days. N = 14 wildtype females, 12 mutant females, 9 wildtype males, 10 mutant males. Data is analyzed using two-way ANOVA.

	wt female	mut female	wt males	mut males	P-value
DD tau	23.89	23.72	23.939	23.84	0.01
DD power	1806.95	1685.19	2189.07	1603.48	0.03
DD act count	41.17	30.75	44.68	38.65	
DD onset	23.89	23.76	23.3	23.87	
DD onset error	0.26	0.34	0.19	0.25	0.04
LD tau	23.92	23.92	23.98	23.98	
LD power	2220.3	1999.21	2440.57	2261.47	
LD activity count	44.84	37.43	43.88	43.07	
n	14	12	9	10	

Figure 2.8. Nmf9 protein is highly conserved in Metazoans. (A)Nmf9 protein homologs exist for all branches of Metazoan save the Urochordates, as well as in certain species of fungi. (B) Sliding window analysis of 14 Nmf9 homologs (blue) verifies known motifs and predicts novel domains where the most highly conserved residues (orange) tend to cluster. Threshold value (red) indicates 25% percentile. (C) The most highly conserved amino acid residues (red box) fall within domain 2, the most highly conserved region. (D) High resolution analysis of domains predicts regions of high functional importance. The 10 highest conserved residues are in orange. Light blue indicates gaps in sequence. Amino acid residues are given for regions of highest conservation. N=53 species for ank domain, derived homolog, 47 for ancestral homolog; 60 for domain 1 derived, 52 for ancestral; 54 for domain 2 derived, 49 for ancestral. dN/dS values calculated using HyPhy.

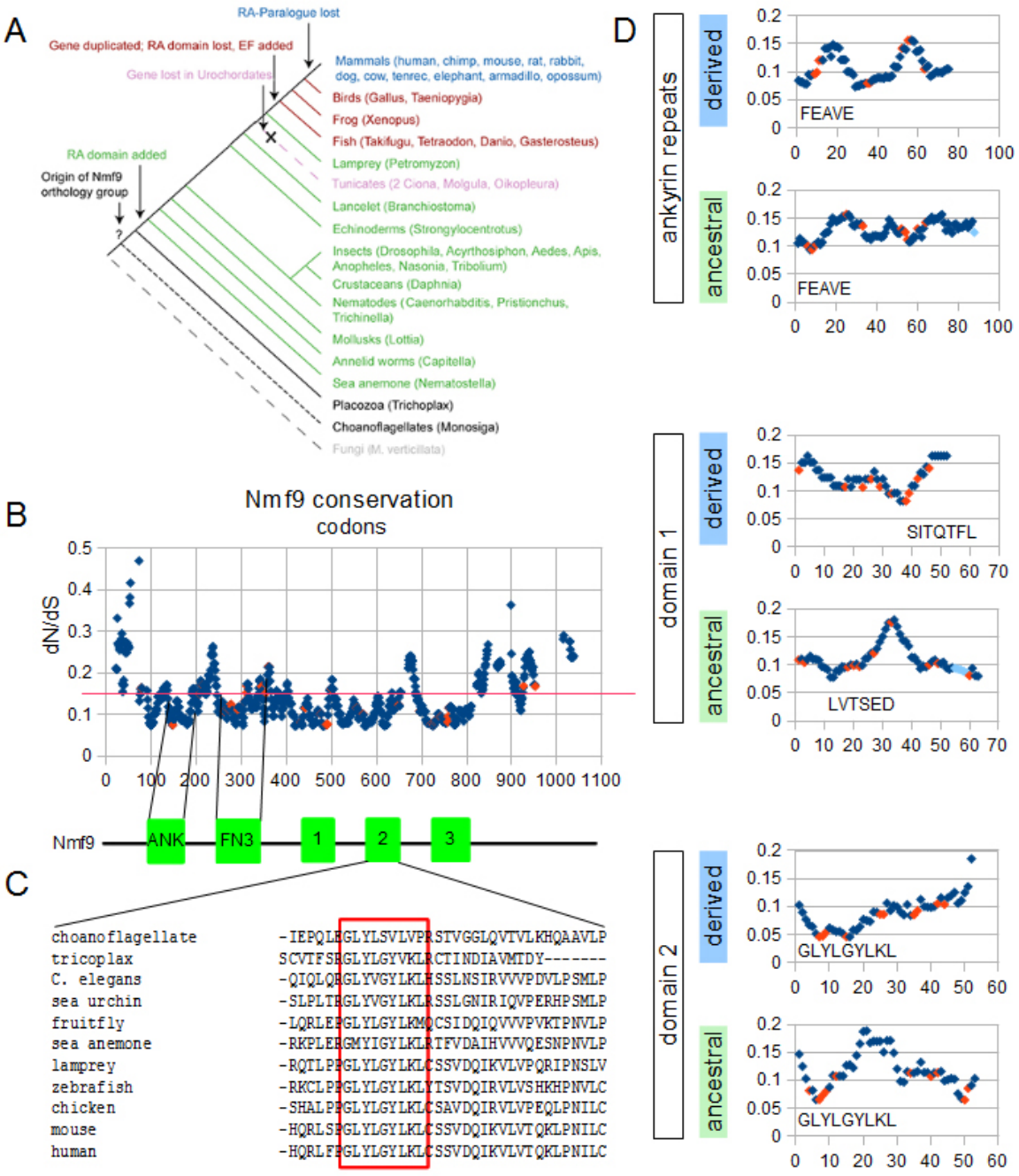
A
RA-Paralogue lost
Gene duplicated; RA domain lost, EF added
Gene lost in Urochordates
RA domain added
Origin of Nmf9 orthology group
?
Mammals (human, chimp, mouse, rat, rabbit, dog, cow, tenrec, elephant, armadillo, opossum)
Birds (Gallus, Taeniopygia)
Frog (Xenopus)
Fish (Takifugu, Tetraodon, Danio, Gasterosteus)
Lamprey (Petromyzon)
Tunicates (2 Ciona, Molgula, Oikopleura)
Lancelet (Branchiostoma)
Echinoderms (Strongylocentrotus)
Insects (Drosophila, Acyrthosiphon, Aedes, Apis, Anopheles, Nasonia, Tribolium)
Crustaceans (Daphnia)
Nematodes (Caenorhabditis, Pristionchus, Trichinella)
Mollusks (Lottia)
Annelid worms (Capitella)
Sea anemone (Nematostella)
Placozoa (Trichoplax)
Choanoflagellates (Monosiga)
Fungi (M. verticillata)
B
Nmf9 conservation
codons
dN/dS
0.5
0.4
0.3
0.2
0.1
0
0 100 200 300 400 500 600 700 800 900 1000 1100
Nmf9
ANK
FN3
1
2
3
C
choanoflagellate -IEPQLEGLYLSVLVPRSTVGGLQVTVLKHQAAVLP
tricoplax SCVTFSRGLYLGYVKLRCTINDIAVMTDY-------
C. elegans -QIQLQRGLYVGYLKLHSSLNSIRVVVPDVLPSMLP
sea urchin -SLPLTRGLYVGYLKLRSSLGNIRIQVPERHPSMLP
fruitfly -LQRLERGLYLGYLKMQCSIDQIQVVVPVKTPNVLP
sea anemone -RKPLERGMYIGYLKLRTFVDAIHVVVQESNPNVLP
lamprey -RQTLPRGLYLGYLKLCSSVDQIKVLVPQRIPNSLV
zebrafish -RKCLPRGLYLGYLKLYTSVDQIRVLVSHKHPNVLC
chicken -SHALPRGLYLGYLKLCSAVDQIRVLVPEQLPNILC
mouse -HQRLSRGLYLGYLKLCSSVDQIKVLVTQKLPNILC
human -HQRLFRGLYLGYLKLCSSVDQIKVLVTQKLPNILC
D
ankyrin repeats
derived
FEAVE
ancestral
FEAVE
domain 1
derived
SITQTFL
ancestral
LVTSED
domain 2
derived
GLYLGYLKL
ancestral
GLYLGYLKL

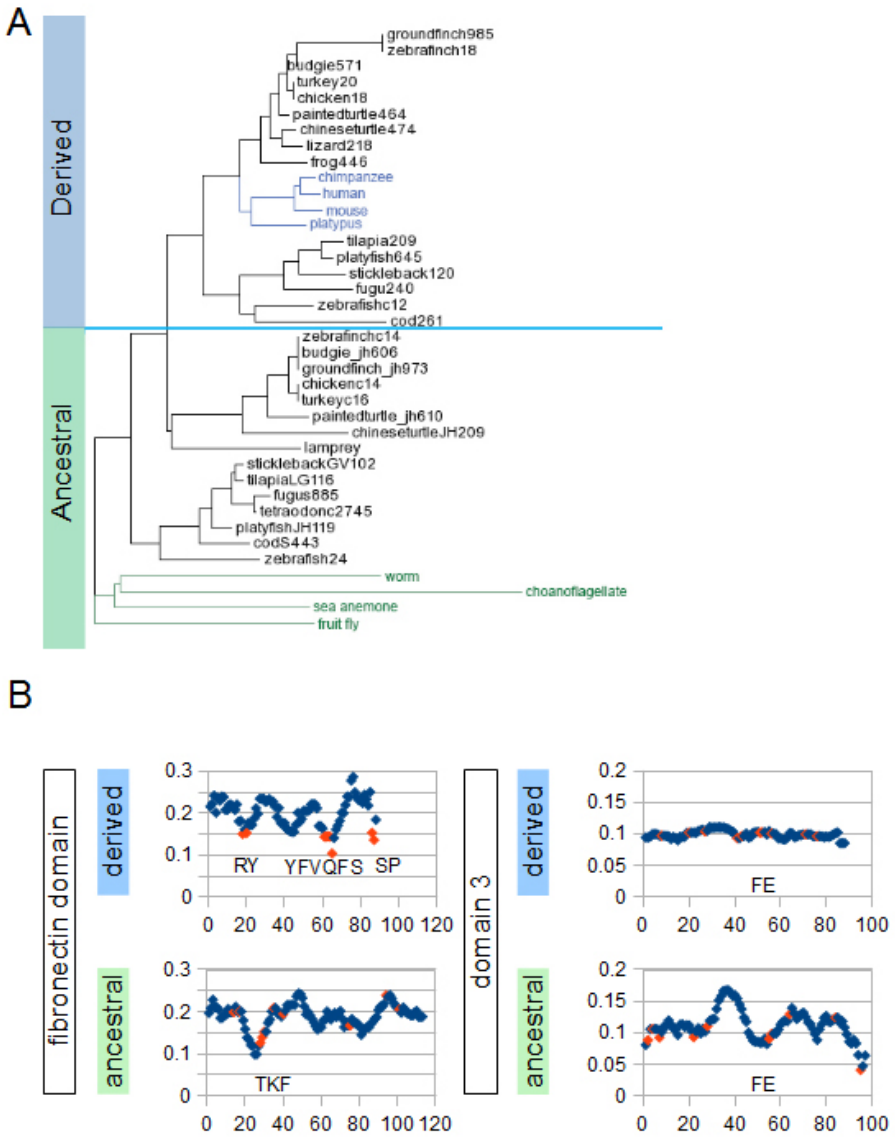

Figure 2.9. *Nmf9* orthologs are more highly conserved in related species than paralogs. (A) In lineages with gene duplication Nmf9 paralogs can be grouped into ancestral and derived versions of the homolog. Phylogenetic trees between homologs were calculated with MUSCLE and plotted using Trex Online. (B) High resolution analysis of 2 conserved domains of Nmf9 protein show different conservation fingerprints between ancestral and derived paralogs across species. The 10 highest conserved residues are in orange. Light blue indicates gaps in sequence. Amino acid residues are given for regions of highest conservation. N=50 species for fn3 derived, 50 for ancestral; 49 for domain 3 derived, 48 for ancestral.

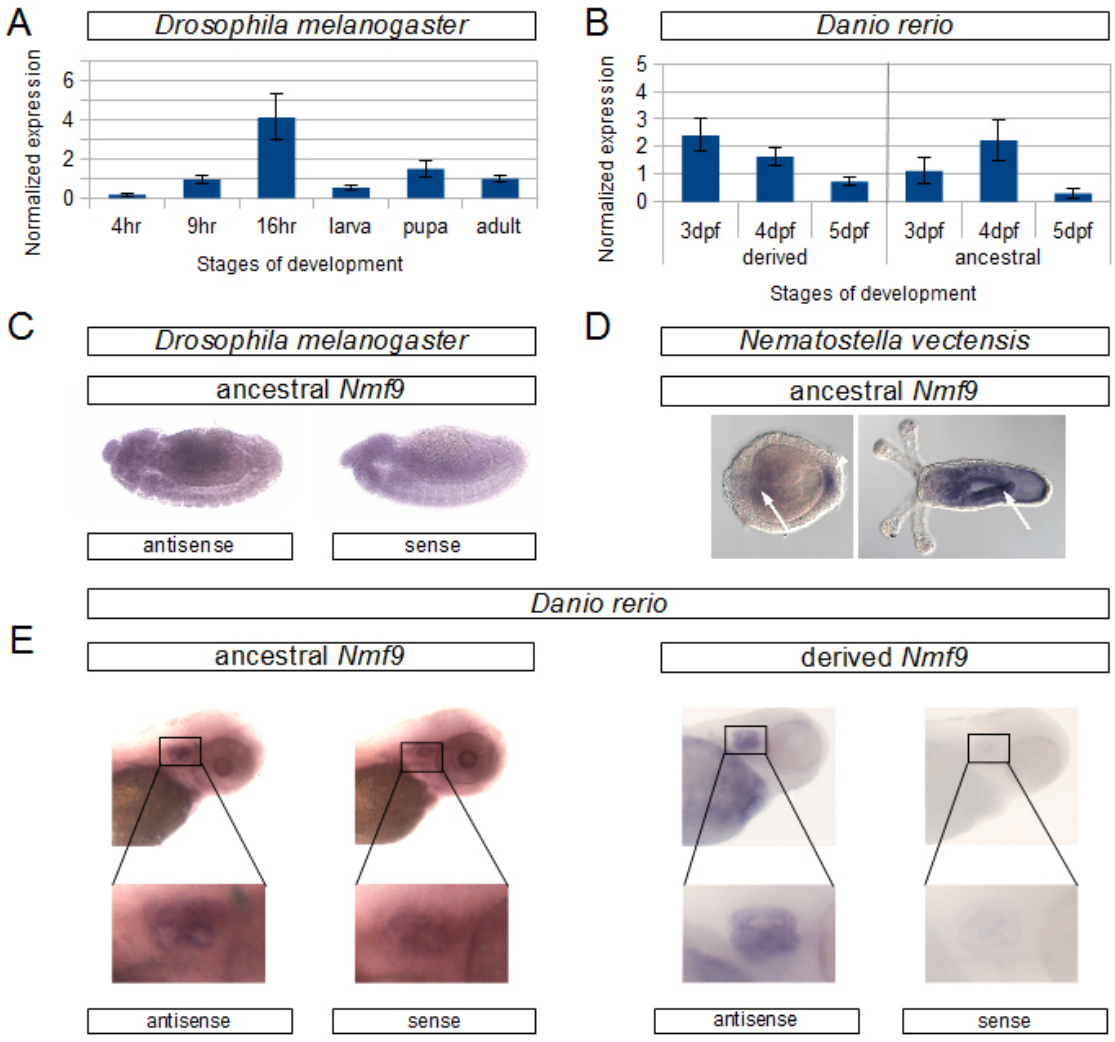

Figure 2.10. Expression of *Nmf9* homologs suggest conservation of function. *Nmf9* is expressed in fruit fly (A) and zebrafish (B) during late development, suggesting conservation of function in development. N=3 technical replicates for zebrafish, 3 biological replicates for fruit fly. (C) *In situ* hybridization shows *Nmf9* enrichment in CNS of fly embryo and (D) in larval sensory cilia (indicated with arrowhead) of sea anemone as well as in septa at both larva and planula stage. (E) Gene duplication results in 2 copies of *Nmf9* in zebrafish, both are expressed in the inner ear.

Table 2.2. Species used in evolution conservation analysis. Homologs of *Nmf9* are identified in various databases and hand curated. Due to quality of the genomes available, sequences that contain more than 50% gaps are removed and not included in this list. Due to poor assembly, all homolog sequences, with the exception of *H. sapiens,* were manually assembled utilizing the BLAST, BLAST, TBLASTN tools available in many of the databases. The ID of the seed sequence is listed when available. Species highlighted in yellow indicate the sequences used in whole-protein conservation analysis. 52 species containing ancestral versions of the homolog and 61 species containing derived versions of the homolog are used for the region specific analysis of conservation.

common name	organism	homolog	identifier
alpaca	Vicugna pacos	derived	ENSVPAG00000010256
anole lizard	Anolis carolinensis	both	ENSACAG00000009106
			ENSACAG00000016399
aphid	Acryrthosiphon pisum	ancestral	XM_003247415.1
armadillo	Dasypus novembinctus	derived	ENSDNOG00000024881
baboon	Papio hamadryas	derived	N/A
beetle	Tribolium castaneum	ancestral	XM_967507.2
budgerigar	Melopsittacus undulatus	both	JH556571.81
bushbaby	Otolemur garnettii	derived	ENSOGAG00000004979
cat	Felis catus	derived	ENSFCAG00000001897
chicken	Gallus gallus	both	ENSGALG00000003105
chimpanzee	Pan troglodytes	derived	ENSPTRG00000009428
Chinese turtle	Pelodiscus sinensis	both	ENSPSIG00000017061
			ENSPSIG00000002850
choanoflagellate	Monosiga brevicollis	ancestral	N/A
cod	Gadus morhua	both	HE567771.4
			HE571238
coelacanth	Latimeria chalumnae	both	ENSLACG00000008414
			ENSLACG00000006593
cow	Bos taurus	derived	ENSBTAG00000021292
deer tick	Ixodes scapularis	ancestral	XM_002435547.1
dog	Canis lupus familiaris	derived	ENSCAFG00000017372
dolphin	Tursiops truncatus	derived	ENSTTRG00000004357
elephant	Loxodonta africana	derived	ENSLAFG00000001242
ferret	Mustela putorius furo	derived	ENSMPUG00000015393
frog	Xenopus tropicalis	both	ENSXETG00000020302
			ENSXETG00000001327
fruit fly	Drosophila mojavenis	ancestral	XM_002001510.1
fruit fly	Drosophila virilis	ancestral	XM_002055973.1
fruit fly	Drosophila grimshawi	ancestral	XM_001993769.1
fruit fly	Drosophila pseudoobscura	ancestral	XM_003736487.1
fruit fly	Drosophila ananasae	ancestral	XM_001953872.1
fruit fly	Drosophila erecta	ancestral	XM_001982206.1
fruit fly	Drosophila yakuba	ancestral	XM_002098289.1

Table 2.2. Species used in evolution conservation analysis, continued.

common name	organism	homolog	identifier
fruit fly	Drosophila melanogaster	ancestral	NM_001260314.
fruit fly	Drosophila sechellia	ancestral	XM_002032203.
fruit fly	Drosophila simulans	ancestral	XM_002104422.
fugu	Takifu rubripes	both	ENSTRUG00000
			ENSTRUG00000
gibbon	Nomascus leucogenys	derived	ENSNLEG00000
gorilla	Gorilla gorilla gorilla	derived	ENSGGOG00000
medium groundn fin	Geospiza fortis	both	JH739985.25
			JH739973.18
guinea pig	Cavia porcellus	derived	ENSCPOG00000
hedgehog	Erinaceus europaeus	derived	ENSEEUG00000
honey bee	Apis mellifera	ancestral	XR_120109.1
horse	Equus caballus	derived	ENSECAG00000
human	Homo sapiens	derived	ENSG000001539
hyrax	Procavia capensis	derived	ENSPCAG00000
kangaroo rat	Dipodomys ordii	derived	ENSDORG00000
lamprey	Petromyzon marinus	ancestral	ENSPMAG0000
leech	Helobdella robusta	ancestral	N/A
louse	Pediculus humanus corporis	ancestral	XM_002427187 .1
macaque	Macaca mulatta	derived	ENSMMUG000
manatee	Trichechus manatus latirostris	derived	JH594660.220
marmoset	Callithrix jacchus	derived	ENSCJAG00000
medaka	Oryzia latipes	both	ENSORLG00000
megabat	Pteropus vampyrus	derived	ENSPVAG00000
microbat	Myotis lucifugus	derived	ENSMLUG0000
mosquito	Anopheles gambiae	ancestral	XM_321358.5
mosquito	Culex quinquefascitus	ancestral	XM_001861405.
mosquito	Aedes aegypti	ancestral	XM_001662701.
mouse	Mus musculus	derived	ENSMUSG0000
mouse lemur	Microcebus murinus	derived	ENSMICG00000
naked mole rat	Heterocephalus glaber	derived	JH602108.590
nematode	Caenorhabditis japonica	ancestral	n/a
nematode	Caenorhabditis briggsae	ancestral	XM_002644730.
nematode	Caenorhabditis elegans	ancestral	R07E4.1a
nematode	Caenorhabditis brenneri	ancestral	n/a
nematode	Caenorhabditis remanei	ancestral	XM_003117930.
opossum	Monodelphis domestica	derived	ENSMODG0000
orangutan	Pongo abelii	derived	ENSPPYG00000
painted turtle	Chrsemys picta bellii	both	JH584464.20 JH584610.17
panda	Ailuropoda melanoleuca	derived	ENSAMEG0000
pig	Sus scrofa	derived	ENSSSCG00000
pika	Ochotona princeps	derived	ENSOPRG00000
platyfish	Xiphophorus maculatus	both	ENSXMAG0000 ENSXMAG0000
platypus	Ornithorhynchus anatinus	derived	ENSOANG0000
polychaete worm	Capitella teleta	ancestral	N/A

Table 2.2. Species used in evolution conservation analysis, continued.

common name	organism	homolog	identifier
rabbit	Orctolagus cuniculus	derived	ENSOCUG00000001342
rat	Rattus norvegicus	derived	ENSRNOG00000002415
sea anemone	Nematostella vectensis	ancestral	XM_001625514.1
sea snail	Lottia gigantea	ancestral	N/A
sea urchin	Strongylocentrotus purpuratus	ancestral	XM_003726382.1
shrew	Sorex araneus	derived	ENSSARG00000008053
silk worm	Bombyx mori	ancestral	BGIBMGA007117-TA
sloth	Choloepus hoffmanni	derived	ENSCHOG00000012184
squirrel	Ictidomys tridecemlineaatus	derived	ENSSTOG00000010280
squirrel monkey	Saimiri boliviensis	derived	JH378149.206
stickleback	Gasterosteus aculeatus	both	ENSGACG00000010120
			ENSGACG00000008256
tarsier	Tarsius syrichta	derived	ENSTSYG00000003762
tasmanian devil	Sarcophilus harrisii	derived	ENSSHAG00000008960
tenrec	Echinops telfairi	derived	ENSETEG00000019030
tetraodon	Tetraodon nigroviridis	both	ENSTNIG00000003573
			ENSTNIG00000012796
tilapia	Oreochromis niloticus	both	ENSONIG00000019082
			ENSONIG00000020029
tree shrew	Tupaia belangeri	derived	ENSTBEG00000015417
trichoplax	Trichoplax adhaerens	ancestral	N/A
turkey	Meleagris gallopavo	both	ENSMGAG00000008338
			ENSMGAG00000009985
wallaby	Macropus eugenii	derived	ENSMEUG00000005081
wasp	Nasonia vitripennis	ancestral	XM_001607671.2
water flea	Daphnia pulex	ancestral	n/a
zebrafinch	Taeniopygia guttata	both	ENSTGUG00000003275
			ENSTGUG00000009513
zebrafish	Danio rerio	both	ENSDARG00000060941
			ENSDARG00000073777

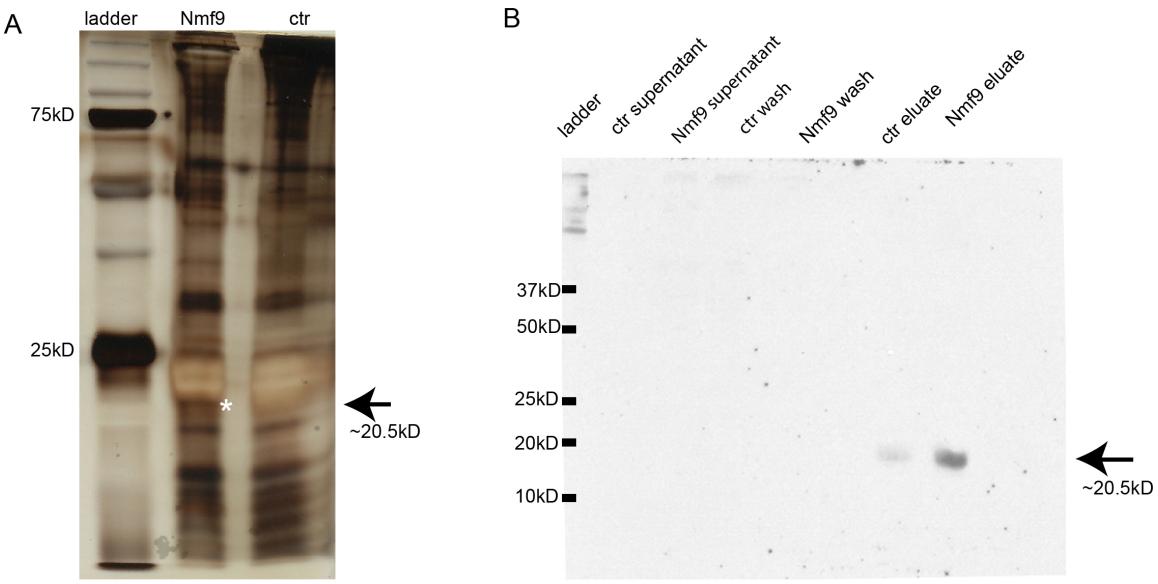

Figure 2.11. Nmf9 interacts with ARF5, a small G protein. (A) Silver stain detects enrichment of a low MW band in cells induced to produce LAP-tagged Nmf9, but not in uninduced control during IP with anti-GFP antibody. (B) Anti-ARF antibody detects low MW band in western blot with of IP with anti-GFP antibody against LAP-tagged Nmf9, but not in LAP tag control.

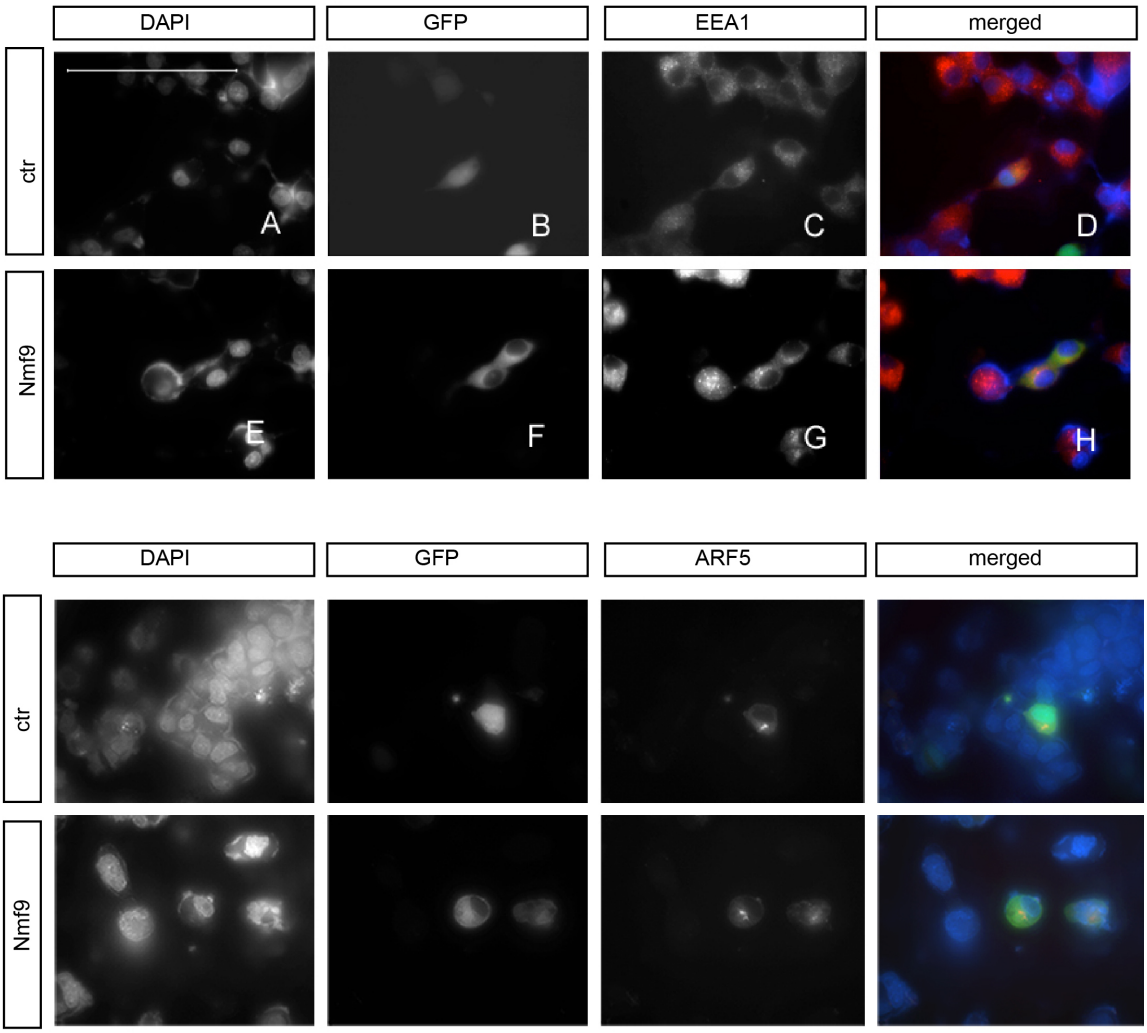

Figure 2.12. Nmf9 is a cytoplasmic protein. (A) GFP-tagged full-length Nmf9 is cytoplasmic and does not co-localize with small cytoplasmic vesicles such as EEA1. (B) No significant co-localization of Nmf9 and ARF5 is detected.

Table 2.3. Oligos used in experiments. In order, the primers used are divided into groups for genotyping, mouse qPCR, fly qPCR, zebrafish qPCR, ISH probe synthesis, and TNT synthesis. The forward genotyping primer is used for sequencing JAX mice, the CRISPR reverse primer is used for sequencing the CRISPR mice. The *Drosophila* qPCR primers will amplify all isoforms of *CG6954,* while the *Danio* qPCR primers are paralog specific.

Oligos

Name	Sequence
Nmf9_10Jul16seq.for	TCCGTCTCTCATTGCCCTAC
Nmf9-Jax.rev	CACATGAGGCCAAGGAAAAT
Nmf9-CRISPR.rev	ttc tga aca tct ctc cgg gg
qPCR_Ank.for	tca aac atc tga aga ggg agg t
qPCR_Ank.rev	cgc ctc tac aca cag gag gt
qPCR_E22.for	cag ctg cag tgt gga gag g
qPCR_E22.rev	aca ttt gaa ggc gtc cta tgg
qPCR_both.for	Taa tcc tta cac ccc gca ct
qPCR_both.rev	Tca gag agt cca gct cca ca
GAPDH	AGAACATCATCCCTGCATCC
GAPDH	ACACATTGGGGGTAGGAACA
pitpA	GCCTGGAATGCCTACCCTTA
pitpA	GTTTATGCACATTCTCCTGG
DM_GAPDH.for	CGAGTTTTCGCCCATAGAAA
DM_GAPDH.rev	ATCGATGAAGGGATCGTTGA
DM_RP49.for	TTCCAGCTTCAAGATGACCA
DM_RP49.rev	GTTCGATCCGTAACCGATGT
DM_all.for	CCAACGACGTAATCCCAAAA
DM_all.rev	TGTGCAAAGCACTCGGATAG
Dr_SDHA.for	atc aga gag gga agg ggt gt
Dr_SDHA.rev	agg tga tga cct gtc cct tg
Danio.ch12b_for	GCAGCGCTCCCGATGTCCTC
Danio.ch12b_rev	CACGAAGCCAGCGGTGTGGT
Danio.ch24_for	CCTGGAGTACCCGCCGACCA
Danio.ch24_rev	CGGCTGCACACGAGCACTGA
Dr_EF1a.for	GTGCTGTGCTGATTGTTGCT
Dr_EF1a.rev	TGTATGCGCTGACTTCCTTG
Ank_ISH1.T3	aat taa ccc tca cta aag gg G CAC GTT GTT GGT CA
Ank_ISH1.T7	taa tac gac tca cta tag gg ATA GGA AGG AGG TTC GC

Table 2.3. Oligos used in experiments, continued.

Name	Sequence
Ank_ISH2.T3	aat taa ccc tca cta aag gg ctg cag gtt atc cat ga
Ank_ISH2.T7	taa tac gac tca cta tag gg TG ACC AAC AAC GTG C
Ank_ISH3.T3	aat taa ccc tca cta aag gg ga gtc atc tat ttc aac aat tgg
Ank_ISH3.T7	taa tac gac tca cta tag gg TC ATG GAT AAC CTG CAG
Ank_ISH4.T3	aat taa ccc tca cta aag gg AAT GTT GTG GTT TTC ACG G
Ank_ISH5.T7	taa tac gac tca cta tag gg c cgt gaa aac cac aac att
Rik_ISH6.T3	aat taa ccc tca cta aag gg act gtc tgt ggg ga
Rik_ISH6.T7	taa tac gac tca cta tag gg CAT TTT TGC AGC TAC AGA G
Rik_ISH7.T3	aat taa ccc tca cta aag gg g ccc atc cac cac a
Rik_ISH7.T7	taa tac gac tca cta tag gg TC CCC ACA GAC AGT G
Rik_ISH8.T3	aat taa ccc tca cta aag gg gcc acc cta aag cat act a
Rik_ISH8.T7	taa tac gac tca cta tag gg t gtg gtg gat ggg c
T3	aat taa ccc tca cta aag gg
T7	taa tac gac tca cta tag gg
Cas9F	TAATACGACTCACTATAGGGAGAATGGACTATAAGGACCA
	CGAC
Cas9R	GCGAGCTCTAGGAATTCTTAC
Nmf9GtoA_target	TTGCCCTACAGGATATTCTGTCCTACCACAAGAGGAGCCAT
	CAGCGGCTCTCACCCGCACTGTATCTAGGTTACCTAAAGCT
	GTGTAGCTCTGTGGATCAG
Nmf9KtoA_target	CTCTCATTGCCCTACAGGATATTCTGTCCTACCACAAGAGG
	AGCCATCAGCGGCTCTCACCCGGACTGTATCTAGGTTACCT
	AGCGCTGTGTAGCTCTGTGGATCAGATCAAAGTGCTCGTAA
	CCCAA
Nmf9YtoA_target	CTCTCATTGCCCTACAGGATATTCTGTCCTACCACAAGAGG
	AGCCATCAGCGGCTCTCACCCGGACTGGCTCTAGGTTACCT
	AAAGCTGTGTAGCTCTGTGGATCAGATCAAAGTGCTCGTAA
	CCCAA

Table 2.4. Plasmid constructs. Constructs are grouped, in order, for expression in mammalian cells, plasmid production in bacteria, and expression in bacteria.

Constructs

Name	Description
pIC113_Nmf9	full length Nmf9 protein with LAP tag (GFP and S protein) on N terminus
pIC113_Ndel1	Nmf9 with N terminus through ankyrin repeats deleted, LAP tag on N terminus
pIC113_Ndel2	Nmf9 with N terminus through fibronectin domains deleted, LAP tag on N terminus
pIC113_Ndel3	Nmf9 with N terminus through conserved domain 1 deleted, LAP tag on N terminus
pIC113_Ndel4	Nmf9 with N terminus through conserved domain 2 deleted, LAP tag on N terminus
pIC113_Cdel1	N terminus and ankyrin repeats of Nmf9, LAP tag on N terminus
pIC113_Cdel2	N terminus through fibronectin domain of Nmf9, LAP tag on N terminus
pIC113_Cdel3	N terminus through conserved domain 1 of Nmf9, LAP tag on N terminus
pIC113_Cdel4	N terminus through conserved domain 2 of Nmf9, LAP tag on N terminus
pIC113_del1	Nmf9 with only ankyrin repeats deleted, LAP tag on N terminus
pIC113_del2	Nmf9 with only fibronectin domain deleted, LAP tag on N terminus
pIC113_del3	Nmf9 with only conserved domain 1 deleted, LAP tag on N terminus
pIC113_del4	Nmf9 with only conserved domain 2 deleted, LAP tag on N terminus
pIC111_mcher_ARF5	ARF5 with mcherry and poly-his tag on C terminus
pIC111_mcher_ARF6	ARF6 with mcherry and poly-his tag on C terminus
pTRE_Nmf9	full length Nmf9 protein with LAP tag on N terminus in tet-on pTRE vector
pTRE_LAP	LAP tag in tet-on pTRE vector
chr12 zebrafish	697 fragment of chr12 homolog in pGEM T-vector
chr24 zebrafish	605bp fragment of chr24 homolog in pBluescript
CG6954	LD15640 full length cDNA in pBluescript SK-
Atoh1	mouse Atoh1 in pBluescript
Nmf9.3/.6-pTrcHis	polyHis tagged Nmf9 fragment, conserved domain 1 through partial domain 3
Nmf9.8/.9-pTrcHis	polyHis tagged Nmf9 fragment, partial domain 3 through putative EF hand
pET_N-term	PolyHis tagged N terminus fragment of Nmf9
pET_C-term	PolyHis tagged C terminus fragment of Nmf9
pET_arf5	PolyHis tagged full-length ARF5
pET_arf6	PolyHis tagged full-length ARF6
pET_mutQ	polyHis tagged full-length ARF5 in GTP-locked form
pET_mutT	polyHis tagged full-length ARF5 in GDP-locked form
TNT_ank-fn3	Nmf9 fragment behind T7 promoter, N-terminus through fn3 domain
TNT_fn3-dom1	Nmf9 fragment behind T7 promoter, fn3 domain through conserved domain 1
TNT_dom1-dom2	Nmf9 fragment behind T7 promoter, conserved domain 1 through 2
TNT_dom2-dom3	Nmf9 fragment behind T7 promoter, conserved domain 2 through C-terminus
TNT_NCS1	Coding sequence for NCS1 gene behind T7 promoter

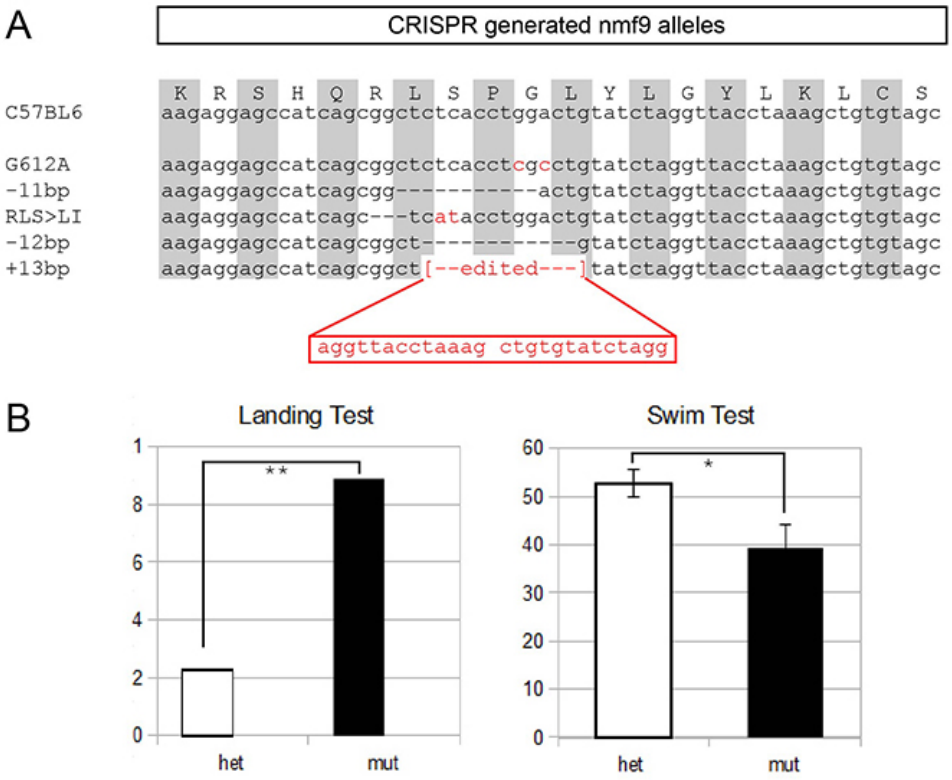

Figure 2.13. CRISPR alleles fail to complement founding *nmf9* allele. (A) CRISPR technology for mutagenesis targeting highly conserved GLYGYLK region in domain 2 generated both the targeted G612A allele as well as additional alleles with small insertions or deletions. (B) Mutant animals carrying various CRISPR alleles over the founding allele show significant impairment of vestibular function compared to their heterozygous littermates. N=30 animals carrying mutant allele over wildtype, N=19 animals carrying one of the CRISPR alleles over JAX allele. P-value <0.001 for Landing Test, analyzed with Fisher's Exact Test. P-value =0.011 for Swim Test, analyzed with two-sample T-Test.

Table 2.5. Summary of vestibular test results in CRISPR-generated mutants. The values indicate number of animals that show mutant phenotype over total number of animals scored for each genotype. Littermates heterozygous for wildtype allele are used as control.

	Heterozygous			Homozygous		
Allele	**Genotype**	**Landing**	**Swim**	**Genotype**	**Landing**	**Swim**
G612A	+/nC	0/5	0/5	nJ/nC	4/5	3/5
-11bp	+/nJ	2/6	2/6	nJ/nC	3/3	1/3
RLS>LI	+/nC	1/7	2/7	nJ/nC	2/2	1/2
-12bp	+/nC	0/3	0/3	nJ/nC	3/4	3/4
+13bp	+/nC	0/2	0/2	nJ/nC	5/5	4/5

Chapter 3: Future Directions and Concluding Remarks

3.1 Summary

Scientists have known since the release of the first mouse genome in 2002 and first human genome in 2003 that, despite technological advancements, we still have very little idea of what many of the genes' functions are. Large scaled screens, be they mutagenesis screens in model organisms or genome-wide analyses of human patients, have led to insights into many novel genes and how they fit into the known pathways and networks. Mutagenesis screens in mice have been particularly valuable due to the genetic similarities between human and mouse. For all large scaled screens, however, there comes a point for each investigator where it is necessary to focus on one or a few genes of interest and perform in depth studies to understand their functions. The functions of many genes have been published to date, but many orphan genes and uncharacterized mutations remain.

Nmf9 was one of these genes of unknown function. It was generated by Jackson Laboratory's mutagenesis screens and preliminary a screen for neurological phenotypes identified the mutant, *nmf9,* which shows tremor and vestibular dysfunction. This suggests that the transcript containing *nmf9* has some function in the nervous system, specifically in the vestibular system, though it does not necessarily limit *Nmf9* to this system. The fact that no auditory dysfunctions were noted at the time suggested that this novel gene may be part of the pathway that differentiates the vestibular system from the auditory system in the inner ear, though they are interconnected compartments that share much of their developmental pathways. The genetics of vestibular dysfunction in

particular has been noted as lacking compared to that of auditory dysfunction, and there is a call for additional research in the vestibular field in order to improve the current standards of diagnoses and treatment (Oh, 2013). The fact that *nmf9* mutants show vestibular dysfunction without noticeable auditory defect positions *Nmf9* as a possible distinguishing factor between the functions of the vestibular and auditory systems. Furthermore, given that the particulars of differentiation between the vestibular and the auditory system are not very well understood, *nmf9* is poised to offer novel insight into the development of the inner ear, beyond what we currently know about *Wnt* signaling in the differentiation pathway (Stevens et al., 2003).

In my work I have found that *Nmf9* is a highly conserved gene that functions at multiple sites in addition to the peripheral vestibular system. I have found that *Nmf9* does indeed serve a vestibular-specific function in the inner ear. It is likely that this function is important for development, since *Nmf9* expression appears to be most enriched in the embryonic vestibular, but not auditory systems. We have identified the novel *Nmf9* transcript and I have found that *Nmf9* is expressed in the hair cell progenitors in the vestibular organs during embryonic development, but not in the cochlea. The adult mutant animals do indeed show vestibular dysfunction as predicted by the preliminary behavioral screen at Jackson Laboratory and by the *in situ* expression data. The vestibular impairment appears to be age-dependent and progressive, though the animals show normal hearing. In addition, I have found that *Nmf9* is also expressed in the neuroproliferative layer in the ventricular zone of the embryo, suggesting a possible path of investigation for the tremor phenotype. The expression of *Nmf9* in adult animals in distinct regions of the brain led to my discovery that *Nmf9,* in addition to the vestibular system, is also important for the functions of the limbic system and the circadian system. Identification of the transcript has also allowed us to take advantage of the bioinformatics

data available and identify Nmf9 as a highly conserved protein, with potential conservation of function in mechanosensory structures throughout the Metazoan lineage. Conservation across the homologs has also allowed us to predict domains important to protein function, and highlighted specific residues to target for further studies with the use of deletion constructs and CRISPR mutagenesis. With CRISPR technology, we have created additional alleles of *nmf9,* not only verifying the identity of the transcript by non-complementation, but also confirming the importance of the amino acid residues we predicted using conservation analysis.

I have identified ARF5, a small G-protein, as the main interaction partner of Nmf9, and that Nmf9's relationship with small G-proteins may be conserved. It is worth noting that both Nmf9 and ARF are highly conserved proteins and that orthologs of ARF have been identified in every branch of Eukaryote (Kahn et al., 2005). Nmf9 protein's interaction with ARF5, as well as the phenotypes of several other ARF-pathway mutants, demonstrate how a fairly ubiquitous vesicle trafficking protein can be adapted in a more system / cell-type specific manner. Studies of Nmf9 homologs, such as CG6954 in fruit flies, tentatively confirm this link between Nmf9 and vesicle trafficking. For instance, Formstecher et al have identified Sec5, a protein necessary for protein trafficking, as a possible interaction partner of CG6954 (Formstecher et al., 2005). Mutation of *Sec5* in fruit fly is shown to be lethal in the larval stage, with disrupted trafficking of proteins to neuronal membranes (Murthy et al., 2003). I have shown that the derived homologs of Nmf9 appear to have a more specialized role in mechanosensation and specific neurocircuits compared to the ancestral homolog. This may be the reason why mutants of CG6954 are not larval-lethal, though their balance defect is severe enough to impair survival in adulthood.

Vestibular dysfunction in mutants often presents together with observable

morphological defects such as absence of one or more components of the inner ear and / or degeneration of cells either within the inner ear itself or in the neurons associated with vestibular function (Gibson et al., 1995; Vrijens et al., 2006; Zheng et al., 2010). In *nmf9* there are no obvious signs of gross morphological defect or degeneration. However, it is possible that there are finer scale anomalies that we have not been able to detect, such as abnormal arrangement of hair cells within the vestibular structures, misshapen hair cells, or defects in sub-cellular components. Mutation of *vesicular glutamate transporter 3*, for example, results in the zebrafish mutant *asteroid,* which has normal hair-bundle morphology but is deaf and shows a balance defect as a result of defect in synaptic vesicle regulation (Obholzer et al., 2008). One way to discover whether synaptic activities or the vesicular trafficking pathway have been affected in *nmf9* mutants is with electron microscopy, though electrophysiology is needed as well in order to discover whether or not the hair cells and afferent nerves present in the mutants are functional.

One of the main difficulties in working with *Nmf9* is that both the transcript and the protein are low in abundance. *Nmf9* is not merely a vestibular gene, and there may be many other systems affected by *Nmf9* that we lack the power to detect. This may be due to the complexities of the phenotypes already present as well as the low abundance of the transcript and protein which make them difficult to work with. For instance, low abundance of the transcript limited our ability to detect additional isoforms. Thus, even though RACE PCR has suggested multiple possible 5-prime ends, we were only able to detect one main isoform in our experiments. Another limitation is that the low abundance of the protein means that, as of the time of this work, no verifiable antibody against Nmf9 protein is available, commercially or otherwise. Even aside from the difficulties of attempting to detect the signal from something that is low abundance, the low

abundance of the protein makes it difficult to develop a working antibody to study the native protein. At this time, it is not yet possible to use immunofluorescence to study the localization of the native protein, or perform pull-down experiments against the native protein to identify its interaction partners in a more natural system. These limitations reduced our ability to screen and identify any possible interaction partners for Nmf9 outside of the epitope-tagged vector expression system. Further screens with the yeast two-hybrid system may be needed to detect low abundance / more transient interaction partners.

Although large-scale screens are an essential tool in identifying genes of interest, ultimately the important biological questions must be addressed on a gene-by-gene basis. This is especially important in mutagenesis screens where novel mutations and sometimes novel genes are identified, where “de-orphanizing” the mutation is necessary to understanding the function of a new gene or uncover previously unsuspected functions of known genes, via new alleles. Even when there is no information regarding a mutation, there can still be a pipeline for how to most effectively conduct a study. Mapping the mutation has become an increasingly rapid process due to advances in technology, and identification of the gene and transcript, even in the absence of previous literature, will still pave the route for studies of mutations. After identification of the transcript, studying the location and timing of expression will suggest roles in function. In addition, function can also be deduced by taking advantage of increasingly more accessible sequencing technology, and therefore the increasing availability of genomes from many organisms besides the classic model organisms. Analysis of possible functions of the homologs may suggest additional functions of the gene of interest, direct further studies in our organism of interest, as well as suggest possible pathways and interaction partners. In the absence of that, sequence information across species is

useful for conservation analyses, which can identify regions important to the function of the gene / protein and is useful for designing targeted deletions. The results of many large-scaled screens still remain in need of “de-orphanization”, and the processes described above are necessary for many of them. There will no doubt be many interesting answers that are worth looking forward to, but in order to find those answers, we must first ask the right questions. It is only once we have linked these orphan genes to a pathway that we can know what the truly interesting, function-related questions might be.

3.2 Future Directions

The dissertation presented here has identified a novel, highly conserved transcript that, when mutated, causes vestibular dysfunction in mice. In the process of studying the function of this gene, many other interesting questions were raised that, while outside the scope of this current work, may be worth pursuing. For instance, the availability of sequence information for a myriad of species, combined with the development of CRISPR technology, made it possible to identify and edit amino acid residues that are important for the functions of the protein. To this end, we have created CRISPR lines in both mice and flies whose genomes have been edited just upstream of the critical regions, resulting in either missense or nonsense transcripts, or have had the critical amino acid residues substituted in-frame. We have shown that mutating the predicted residues in mice will indeed result in mutants that fail to complement the JAX *nmf9* mutants and that these CRISPR mutants show similar vestibular phenotypes. However, further behavioral studies may be needed in order to discover if these predicted residues are as critical to the functions of SCN and AMY as they are to the function of the inner ear in mice.

There are many questions still unanswered regarding the CRISPR fruit fly mutants and their phenotype. We do not yet know whether their circadian functions or olfaction are affected, though we do know the *Drosophila* Nmf9 protein homolog has been detected in the antenna of fruit flies (Anholt and Williams, 2010) and that fly antennae are important both for olfaction and mechanosensation. Mutations just upstream of the highly conserved region in domain 2 results in fly mutants that show uncoordinated behavior and inability to remain upright similar to mechanosensory mutants such as *NOMPC* (Zhang et al., 2013). *Nmf9 Drosophila* mutants die within a week of emerging from pupa and have wings that are grossly normal, though they are

unable to fly. Additional study is needed to discover whether the mechanosensory phenotype in these mutants is balance-specific, or if the auditory and tactile systems are affected as well.

Another direction for future studies is the ARF pathway. ARF proteins can switch between the active, GTP-bond form and the inactive, GDP-bond form. The switch between the two forms is a tightly regulated process that requires GEFs and GAPs, and the active and inactive forms are important to different signal pathways downstream that regulate vesicle assembly and cargo packaging (D'Souza-Schorey and Chavrier, 2006). Class II ARFs are not as well studied as either class I or III, though enough is known about ARF5 that mutants permanently locked in either GTP-bond or GDP-bond form have been created. Future studies to determine whether Nmf9 shows a preference for interaction with either the GTP-bond form or GDP-bond form of ARF5 would determine whether Nmf9 is part of the activating or inhibitory pathway. They would also provide additional insights regarding the functions of ARFs, since class II ARFs have never been implicated in vestibular functions. Potential future experiments include using electron-microscopy to determine whether there is a build-up of vesicles or abnormal vesicle morphology. These types of cell abnormalities are commonly associated with defects in protein trafficking, such as the *vglut3* mutant (Obholzer et al., 2008). The pH of the vesicles could also be assessed, as suggested by Martina et al (Martina et al., 2010), and immunofluorescence coupled with flow cytometry can be used to assay protein internalization and trafficking at the plasma membrane. Since the domains important to Nmf9 protein function are known, it would be worthwhile to conduct trafficking studies with mutant cells expressing either full-length constructs or constructs containing deletion of these domains. Since there is more than one highly conserved domain, it is possible that each domain will serve a different role in the binding-signaling cascade.

Analysis of the different constructs may reveal which domain is essential for binding to ARF5 and which is essential for initiating downstream signaling.

There are more general questions which remain regarding the relationship between Nmf9 and small G proteins, especially regarding their roles in the circadian pathway. Small G proteins have been tentatively linked to the functions of the circadian system in the past. ARF1 has been linked to circadian rhythm in green algae as early as 1995 (Memon et al., 1995), and a more recent paper detects ARF5 as one of the proteins in mouse liver that appears to be driven by circadian rhythm and identifies RAB1, another small G protein, as showing circadian oscillation (Robles et al., 2014). These results raise the possibility that ARF5 may function as a part of a feedback loop in circadian systems. Future experiments examining the expression of Nmf9 and ARF5 on a finer time scale for circadian oscillation, as well as Yeast Two-Hybrid screens for less abundant, more transient protein interaction partners, may uncover the importance of Nmf9 protein in the SCN.

There are questions regarding the role of Nmf9 in the other associated nuclei as well. It is unknown whether Nmf9 operates in similar protein interaction networks in the various nuclei in the adult brain as it does in the inner ear. If Nmf9 results in a more ubiquitous dysfunction in neurons via protein trafficking, then the question becomes why dysfunction is detected only in some, but not all, of the nuclei expressing *Nmf9*. Comparison of *Nmf9* function between the affected systems (SCN, AMY) and the unaffected systems (LS, PC, VMH) may yield insight as to why certain neurocircuits are more sensitive to perturbation than others. Developing an antibody that recognizes the endogenous protein in tissue to perform additional studies with various cell markers, may identify the cell type that expresses Nmf9 and sub-populations of neurons that are necessary for accurate functions of SCN and AMY. This, in turn, may provide clues to

pathways and functions that distinguish those particular neurons from their neighbors.

Lastly, the cause of tremor observed in *nmf9* mutants remained largely unstudied in this work, though we have observed no obvious defects in myelination nor degeneration that are usually present in mutants with this phenotype. The expression of *Nmf9* transcript in the ventricular zone (VZ) during embryonic stages in mice, specifically in the lateral and medial ganglionic eminences, suggests that *Nmf9* may play a role in interneuron proliferation or migration. Though no *Nmf9* expression is detected in neuroproliferative zones in adult tissues, its expression in VZ during development provides a potential link between the *nmf9* mutation and the observed tremor. More detailed study of the neuroanatomy, such as examination of dendritic and synaptic morphology, as well as quantification of cortex size and examination of cortical layer organization, would reveal whether neuroproliferation and migration in the embryo has been affected. The ganglionic eminences are known sources of GABAergic interneurons (Lavdas et al., 1999; Taglialatela et al., 2004), and quantification with immunofluoresence may reveal a depletion of this particular cell type in nmf9 mutants.

3.3 Concluding Remarks

In my thesis work I have identified *nmf9 a*s a mutation that induces a splicing error in a low-abundance transcript that is often misannotated. I have linked the point mutation to the observed phenotype in the animals by determining the location and time of expression of the novel transcript, which allowed me to predict and test for functional impairment of additional neurocircuits that were not obvious during the initial screen. In addition, I have identified ARF5 as an interaction partner with the Nmf9 protein, placing the novel gene into a known protein network, and providing the first link between class II ARFs and vestibular dysfunction, thus de-orphanizing the *Nmf9* gene. Finally, I have identified protein regions that are important for the functions of Nmf9, including specific amino acids critical to Nmf9 that, when mutated in mice, will recapitulate the original phenotype. All of these contributions suggest that the pathways involving class II ARFs, like those that involve class I and class III ARFs, are critical to the function of the peripheral vestibular system. Furthermore, they suggest that class II ARFs can be important to the function of specific subgroups of neurons in the brain. My work predicts that *nmf9* mutants may have impaired protein trafficking and suggests that the function of *Nmf9* may be conserved at least as far back as *Drosophila*. As the function of ARFs in neurons and especially the inner ear become more clearly defined in the future, we will gradually uncover the missing pieces in vestibular genetics, with an eye toward improving the diagnoses and treatment of vestibulopathies in years to come.

Appendix: Protocols

A.1: Protocol for Sodium Hydroxide Extraction of Mouse Tail DNA

DNA used in genotyping of mice are extracted by digesting tail snip sample collected when the animals are around two weeks of age in 600uL of 0.05M sodium hydroxide at 86C for 3 hours. The samples are then neutralized with 50uL of 1M Tris-chloride and vortexed. 1uL of this is used per 15uL PCR reaction.

A.2: Protocol for RNA Extraction

Extraction of RNA for synthesis of cDNA in qRT-PCR is performed using Trizol (Life Technologies), based on directions from the reagent.

Briefly, mouse tissue is dissected into appropriate volume of Trizol reagent and homogenized with a polytron, centrifuged to collect cell debris. After brief incubation at room temperature, 1/5 volume of chloroform is added and the samples shaken vigorously and incubated briefly at room temperature before centrifugation. RNA is then extracted from the aqueous phase with ½ volume isopropanol by shaking the sample and incubating at room temperature then centrifuging. The RNA pellet is rinsed once with 75% ethanol and air dried before redissolving in nuclease free water.

Fly and fish samples are homogenized in Trizol with a pellet pestle and similarly extracted. Fly RNA is extracted with 100% ethanol instead of isopropanol and incubated on ice.

A.3: Protocol for Quantitative Real-Time PCR of *Nmf9* and Homologs

For qRT-PCR, cDNA is synthesized from extracted RNA and diluted to 20ng/uL. Primers are tested for non-specific product amplification with both no-reverse-transcription control and water up to 40 cycles of PCR. 20uL reactions with 2x SYBR Green mix are used. All reactions are set up in technical triplicates on a 96 well plate and results normalized to at least two positive controls (see table 2.3 for list of control primers).

A.4: Protocol for Creating Stable Tet-on Cell Lines

P19 cells are seeded into a 6 well plate and grown until 70-80% confluent. Transfect half of the wells with 5ug of pTet plasmid (ClonTech). At 24 hours post-transfection the cells are rinsed with PBS. 0, 400, and 800ug/mL G418 is added to each of the three transfected and untransfected wells, with the untransfected as control, to find the optimal concentration of selection media. The media is changed with fresh selection reagent every three days until a pair of transfected vs untransfected wells is found where there are no survivers in the untransfected well and healthy colonies in the transfected well. Passage colonies into 10cm plate and continue selection, refreshing media every three days, for at least one month for stable integration.

Repeat process of seeding pTET-P19 cells into a 6 well plate and transfecting half of the wells with pTRE (ClonTech) construct containing gene of interest, test selection with hygromycin. After the plasmid has been stably integrated, grow 1 plate of cell to confluency before trypsinizing the cells. To select single cell colony, perform serial dilution with the pTRE-pTet cells in a 96 well plate, first diluting the suspended cells in 1:2 series down the rows and then diluting the first column in a series of 1:2 dilution across the columns in selection media. Select wells that contain only a single cell colony and expand those wells. Perform test-induction with doxycylin to pick the cell line expanded from single cell colony that has the best expression.

A.5: Protocol for Generating CRISPR Mutants in Mice

Cas9 mRNA and sgRNA production. mRNA for CRISPR targeting is synthesized following the procedure of Wang et al 2013. (Wang et al., 2013) Briefly, Cas9 is amplified by PCR from pX330-U6-Chimeric_BB-CBh-hSpCas9 (Addgene #43220) and transcribed using the mMessage mMachine T7 Ultra Kit (Life Technologies). T7 or Sp6 DNA templates are synthesized as single template strand oligonucleotides (Ultramers, IDT) and amplified for 20 cycles using PfuUltra II Fusion HS DNA Polymerase (Agilent). Transcription is performed using MEGAshortscript T7 and Sp6 Kits (Life Technologies). All samples are purified with MEGAclear Kit (Technologies), eluted in embryo-qualified water (Sigma-Aldrich), and their quality assessed with both denaturing gel electrophoresis and OD 260/280.

Homology-dependent repair. Oligonucleotides with ~60 base arms flanking the desired base changes are synthesized by IDT (Ultramers, IDT). Unpurified oligonucleotides are used directly in injection cocktails according to the manufacturer's concentration.

References

Afifi, A., and Bergman, R. (2005). Functional Neuroanatomy (McGraw-Hill Medical).

Agnostaras, S., Craske, M., and Fanselow MS (1999). Anxiety: at the intersection of genes and experience. Nat. Neurosci. 2, 780–782.

Agrawal, Y., Carey, J.P., Della Santina, C.C., Schubert, M.C., and Minor, L.B. (2009). Disorders of balance and vestibular function in US adults. Arch Intern Med 169, 938–944.

Alcaraz, W.A., Gold, D.A., Raponi, E., Gent, P.M., Concepcion, D., and Hamilton, B.A. (2006). Zfp423 controls proliferation and differentiation of neural precursors in cerebellar vermis formation. Proc. Natl. Acad. Sci. U. S. A. 103, 19424–19429.

Anholt, R.R.H., and Williams, T.I. (2010). The soluble proteome of the Drosophila antenna. Chem. Senses 35, 21–30.

Armbruster, K., and Luschnig, S. (2012). The Drosophila Sec7 domain guanine nucleotide exchange factor protein Gartenzwerg localizes at the cis-Golgi and is essential for epithelial tube expansion. J. Cell Sci. 125, 1318–1328.

Artimo, P., Jonnalagedda, M., Arnold, K., Baratin, D., Csardi, G., de Castro, E., Duvaud, S., Flegel, V., Fortier, A., Gasteiger, E., Grosdidier, A., Hernandez C., Ioannidis, V., Kuznetsov, D., Liechti, R., Moretti, S., Mostaguir, K., Redaschi, N., Rossier, G., Xenarios, I., Stockinger, H. (2012). ExPASy: SIB bioinformatics resource portal. Nucleic Acids Res. 40, W597–603.

Avidor-Reiss, T., Maer, A.M., Koundakjian, E., Polyanovsky, A., Keil, T., Subramaniam, S., and Zuker, C.S. (2004). Decoding Cilia Function : Defining Specialized Genes Required for Compartmentalized Cilia Biogenesis. Cell 117, 527–539.

Bánfi, B., Malgrange, B., Knisz, J., Steger, K., Dubois-Dauphin, M., and Krause, K.-H. (2004). NOX3, a superoxide-generating NADPH oxidase of the inner ear. J. Biol. Chem. 279, 46065–46072.

Beitz, A., and Anderson, J.H. (2000). Neurochemistry of the vestibular system (CRC).

Ben-Arie, N., Hassan, B.A., Bermingham, N.A., Malicki, D.M., Armstrong, D., Matzuk, M., Bellen, H.J., and Zoghbi, H.Y. (2000). Functional conservation of atonal and Math1 in the CNS and PNS. Development 127, 1039–1048.

Bermingham, N.A. (1999). Math1: An Essential Gene for the Generation of Inner Ear Hair Cells. Science 284, 1837–1841.

Beutler, B., Du, X., and Xia, Y. (2007). Precis on forward genetics in mice. Nat. Immunol. 8, 659–664.

Bird, M.T., Shuttleworth, E., Koestner, A., and Reinglass, J. (1971). The wobbler mouse mutant: an animal model of hereditary motor system disease. Acta Neuropathol. 19, 39–50.

De Boer, S.F., and Koolhaas, J.M. (2003). Defensive burying in rodents: ethology, neurobiology and psychopharmacology. Eur. J. Pharmacol. 463, 145–161.

Brooker, R., Hozumi, K., and Lewis, J. (2006). Notch ligands with contrasting functions: Jagged1 and Delta1 in the mouse inner ear. Development 133, 1277–1286.

Burge, C.B., and Karlint, S. (1998). Finding the genes in genomic DNA. Curr. Opin. Struct. Biol. 8, 346–354.

Cai, X., and Zhang, Y. (2006). Molecular evolution of the ankyrin gene family. Mol. Biol. Evol. 23, 550.

Clements, W.K., Kim, A.D., Ong, K.G., Moore, J.C., Lawson, N.D., and Traver, D. (2011). A somitic Wnt16/Notch pathway specifies haematopoietic stem cells. Nature 474, 220–224.

Concepcion, D., Flores-Garcia, L., and Hamilton, B.A. (2009). Multipotent genetic suppression of retrotransposon-induced mutations by Nxf1 through fine-tuning of alternative splicing. PLoS Genet. 5, e1000484.

Contarino, A., Baca, L., Kennelly, A., and Gold, L.H. (2002). Automated assessment of conditioning parameters for context and cued fear in mice. Learn. Mem. 9, 89–96.

Crawley, J.N. (1999). Behavioral phenotyping of transgenic and knockout mice: experimental design and evaluation of general health, sensory functions, motor abilities, and specific behavioral tests. Brain Res. 835, 18 – 26.

Crawley, J.N. (2008). Behavioral phenotyping strategies for mutant mice. Neuron 57, 809–818.

D’Souza-Schorey, C., and Chavrier, P. (2006). ARF proteins: roles in membrane traffic and beyond. Nat. Rev. Mol. Cell Biol. 7, 347–358.

Davidson, A.E., Schwarz, N., Zelinger, L., Stern-Schneider, G., Shoemark, A., Spitzbarth, B., Gross, M., Laxer, U., Sosna, J., Sergouniotis, P.I., Waseem, N.H., Wilson, R., Kahn, R.A., Plagnol, V., Wolfrum, U., Banin, E., Hardcastle, A.J., Cheetham, M.E., Sharon, D., Webster, A.R. (2013). Mutations in ARL2BP, encoding ADP-ribosylation-factor-like 2 binding protein, cause autosomal-recessive retinitis pigmentosa. Am. J. Hum. Genet. 93, 321–329.

Desmond, A. (2004). Vestibular function: evaluation and treatment (Thieme).

Donaldson, J.G., and Jackson, C.L. (2011). Arf Family G Proteins and their regulators: roles in membrane transport, development and disease. Nat. Rev. Mol. Cell Biol. 12, 362–375.

Duijsings, D., Lanke, K.H.W., van Dooren, S.H.J., van Dommelen, M.M.T., Wetzels, R., de Mattia, F., Wessels, E., and van Kuppeveld, F.J.M. (2009). Differential membrane association properties and regulation of class I and class II Arfs. Traffic 10, 316–323.

Eddison, M., Le Roux, I., and Lewis, J. (2000). Notch signaling in the development of the inner ear: lessons from Drosophila. Proc. Natl. Acad. Sci. U. S. A. 97, 11692–11699.

Edgar, R.C. (2004). MUSCLE: multiple sequence alignment with high accuracy and high throughput. Nucleic Acids Res. 32, 1792–1797.

Eugène, D., Deforges, S., Vibert, N., and Vidal, P.-P. (2009). Vestibular critical period, maturation of central vestibular neurons, and locomotor control. Ann. N. Y. Acad. Sci. 1164, 180–187.

Finn, R.D., Mistry, J., Tate, J., Coggill, P., Heger, A., Pollington, J.E., Gavin, O.L., Gunasekaran, P., Ceric, G., Forslund, K., et al. (2010). The Pfam protein families database. Nucleic Acids Res. 38, D211–22.

Fitzgerald, L.W., Miller, K.J., Ratty, A.K., Glick, S.D., Teitler, M., and Gross, K.W. (1992). Asymmetric elevation of striatal dopamine D2 receptors in the chakragati mouse: neurobehavioral dysfunction in a transgenic insertional mutant. Brain Res. 580, 18–26.

Fontaine, C., Dubois, G., Duguay, Y., Helledie, T., Vu-Dac, N., Gervois, P., Soncin, F., Mandrup, S., Fruchart, J.-C., Fruchart-Najib, J., Staels, B. (2003). The orphan nuclear receptor Rev-Erbalpha is a peroxisome proliferator-activated receptor (PPAR) gamma target gene and promotes PPARgamma-induced adipocyte differentiation. J. Biol. Chem. 278, 37672–37680.

Formstecher, E., Aresta, S., Collura, V., Hamburger, A., Meil, A., Trehin, A., Reverdy, C., Betin, V., Maire, S., Brun, C., Jacq, B., Arpin, M., Bellaiche, Y., Bellusci, S., Benaroch, P., Bornens, M., Chanet, R., Chavrier, P., Delattre, O., Doye, V., Fehon, R., Faye, G., Galli, T., Girault, J.-A., Goud, B., de Gunzburg, J., Johannes, L., Junier, M.-P., Mirouse, V., Mukherjee, A., Papadopoulo, D., Perez, F., Plessis, A., Rossé, C., Saule, S., Stoppa-Lyonnet, D., Vincent, A., White, M., Legrain, P., Wojcik, J., Camonis, J., Daviet, L. (2005). Protein interaction mapping: A Drosophila case study. Genome Res. 15, 376 – 384.

Freyer, L., Aggarwal, V., and Morrow, B.E. (2011). Dual embryonic origin of the mammalian otic vesicle forming the inner ear. Development 138, 5403–5414.

Gibson, F., Walsh, J., Mburu, P., Varela, A., Brown, K., Antonio, M., Beisel, K., Steel, K., and Brown, S. (1995). A type VII myosin encoded by the mouse deafness gene shaker-1. Nature 374, 62–64.

Gorman, M.R. (2006). Phase Angle Difference Alters Coupling Relations of Functionally Distinct Circadian Oscillators Revealed by Rhythm Splitting. J. Biol. Rhythms 21, 195–205.

Gupta, R., and Brunak, S. (2002). Prediction of glycosylation across the human proteome and the correlation to protein function. Pacific Symp. Biocomput. 7, 310–322.

Hans, S., Liu, D., and Westerfield, M. (2004). Pax8 and Pax2a function synergistically in otic specification, downstream of the Foxi1 and Dlx3b transcription factors. Development 131, 5091–5102.

Hardisty-Hughes, R.E., Parker, A., and Brown, S.D.M. (2010). A hearing and vestibular phenotyping pipeline to identify mouse mutants with hearing impairment. Nat. Protoc. 5, 177–190.

Holmes, S., and Padgham, N.D. (2011). A review of the burden of vertigo. J. Clin. Nurs. 20, 2690–2701.

Hopitzan, A.A., Baines, A.J., and Kordeli, E. (2006). Molecular Evolution of Ankyrin: Gain of Function in Vertebrates by Acquisition of an Obscurin/Titin-Binding–Related Domain. Mol. Biol. Evol. 23, 46.

Hotz, V.M., King, David P, Chang, Annie-Marie, Kornhauser, Jon M, Lowrey, Phillip L, McDonald, J David, Dove, William F, Pinto, Lawrence H, Turek, Fred W, and Takahashi, Joseph S (1994). Mutagenesis and mapping of a mouse gene, Clock, esential for circadian behavior. Science (80-.). 264, 719–724.

Humphreys, D., Liu, T., Davidson, A.C., Hume, P.J., and Koronakis, V. (2012). The Drosophila Arf1 homologue Arf79F is essential for lamellipodium formation. J. Cell Sci. 125, 5630–5635.

Itoh, M., and Chitnis, A.B. (2001). Expression of proneural and neurogenic genes in the zebrafish lateral line primordium correlates with selection of hair cell fate in neuromasts. Mech. Dev. 102, 263–266.

Jayasena, C., Ohyama, T., Segil, N., and Groves, A. (2008). Notch signaling augments the canonical Wnt pathway to specify the size of the otic placode. Development 135, 2251–2261.

Jen, J.C. (2008). Recent advances in the genetics of recurrent vertigo and vestibulopathy. Curr. Opin. Neurol. 21, 3–7.

Jeon, S.-J., Fujioka, M., Kim, S.-C., and Edge, A.S.B. (2011). Notch signaling alters sensory or neuronal cell fate specification of inner ear stem cells. J. Neurosci. 31, 8351–8358.

Johnson, K.R., Cook, S.A., Erway, L.C., Matthews, A.N., Sanford, L.P., Paradies, N.E.,

and Friedman, R.A. (1999). Inner Ear and Kidney Anomalies Caused by IAP Insertion in an Intron of the Eya1 Gene in a Mouse Model of BOR Syndrome. Hum. Mol. Genet. 8, 645–653.

Johnson, K.R., Longo-Guess, C.M., and Gagnon, L.H. (2012). Mutations of the mouse ELMO domain containing 1 gene (Elmod1) link small GTPase signaling to actin cytoskeleton dynamics in hair cell stereocilia. PLoS One 7, e36074.

Justice, M.J., Noveroske, J.K., Weber, J.S., Zheng, B., and Bradley, A. (1999). Mouse ENU mutagenesis. Hum. Mol. Genet. 8, 1955–1963.

Kahn, R.A, Volpicelli-Daley, L., Bowzard, B., Shrivastava-Ranjan, P., Li, Y., Zhou, C., and Cunningham, L. (2005). Arf family GTPases: roles in membrane traffic and microtubule dynamics. Biochem. Soc. Trans. 33, 1269–1272.

Keithley, E.M., Erkman, L., Bennett, T., Lou, L., and Ryan, A.F. (1999). Effects of a hair cell transcription factor, Brn-3 .1 , gene deletion on homozygous and heterozygous mouse cochleas in adulthood and aging. Hear. Res. 134, 71–76.

Kelley, M.W. (2006). Regulation of cell fate in the sensory epithelia of the inner ear. Nat. Rev. Neurosci. 7, 837–849.

Khan, Z., Carey, J., Park, H.J., Lehar, M., Lasker, D., and Jinnah, H.A. (2004). Abnormal motor behavior and vestibular dysfunction in the stargazer mouse mutant. Neuroscience 127, 785 – 796.

Kiernan, A.E., Ahituv, N., Fuchs, H., Balling, R., Avraham, K.B., Steel, K.P., and Hrabé de Angelis, M. (2001). The Notch ligand Jagged1 is required for inner ear sensory development. Proc. Natl. Acad. Sci. U. S. A. 98, 3873.

Kiernan, A.E., Pelling, A.L., Leung, K.K.., Tang, A.S.., Bell, D.M., Tease, C., Lovell-Badge, R., Steel, K.P., and Cheah, K.S. (2005). Sox2 is required for sensory organ development in the mammalian inner ear. Nature 434, 1031–1035.

Kiernan, A.E., Xu, J., and Gridley, T. (2006). The Notch ligand JAG1 is required for sensory progenitor development in the mammalian inner ear. PLoS Genet. 2, e4.

King, B.M. (2006). The rise, fall, and resurrection of the ventromedial hypothalamus in the regulation of feeding behavior and body weight. Physiol. Behav. 87, 221–244.

King, N., Westbrook, M.J., Young, S.L., Kuo, A., Abedin, M., Chapman, J., Fairclough, S., Hellsten, U., Isogai, Y., Letunic, I., et al. (2008). The genome of chanoflagellate Monosiga brevicollis and the origin of metazoans. Nature 451, 783–788.

Kosakovsky Pond, S.L., Scheffler, K., Gravenor, M.B., Poon, A.F.Y., and Frost, S.D.W. (2010). Evolutionary Fingerprinting of Genes. Mol. Biol. Evol. 27, 520 –536.

Lanford, P.J., Lan, Y., Jiang, R., Lindsell, C., Weinmaster, G., Gridley, T., and Kelley, M.W. (1999). Notch signalling pathway mediates hair cell development in mammalian

cochlea. Nat. Genetics 21, 289–292.

Lavdas, A.A., Grigoriou, M., Pachnis, V., and Parnavelas, J.G. (1999). The medial ganglionic eminence gives rise to a population of early neurons in the developing cerebral cortex. J. Neurosci. 19, 7881–7888.

Lempert, T., and Neuhauser, H. (2009). Epidemiology of vertigo, migraine and vestibular migraine. J. Neurol. 256, 333–338.

Lessenich, A., Lindemann, S., Richter, A., Hedrich, H.J., Wedekind, D., Kaiser, A., and Loscher, W. (2001). A novel black-hooded mutant rat (ci3) with spontaneous circling behavior but normal auditory and vestibular functions. Neuroscience 107, 615–628.

Letunic, I., Doerks, T., and Bork, P. (2009). SMART 6: recent updates and new developments. Nucleic Acids Res. 37, D229–32.

Marlow, H., Roettinger, E., Boekhout, M., and Martindale, M.Q. (2012). Functional roles of Notch signaling in the cnidarian Nematostella vectensis. Dev. Biol. 362, 295–308.

Martina, J.A., Lelouvier, B., and Puertollano, R. (2010). The calcium channel mucolipin-3 is a novel regulator of trafficking along the endosomal pathway. Traffic 10, 1143–1156.

Memon, A.R., Hwang, S., Deshpande, N., Thompson, G.A., and Herrin, D.L. (1995). Novel aspects of the regulation of a cDNA (Arf1) from Chlamydomonas with high sequence identity to animal ADP-ribosylation factor 1. Plant Mol. Biol. 29, 567–577.

Menard, J., and Treit, D. (1996). Lateral and medial septal lesions reduce anxiety in the plus-maze and probe-burying tests. Physiol. Behav. 60, 845 – 853.

Millimaki, B.B., Sweet, E.M., Dhason, M.S., and Riley, B.B. (2007). Zebrafish atoh1 genes: classic proneural activity in the inner ear and regulation by Fgf and Notch. Development 134, 295–305.

Monigatti, F., Gasteiger, E., Bairoch, A., and Jung, E. (2002). The Sulfinator: predicting tyrosine sulfation sites in protein sequences. Bioinformatics 18, 769–770.

Moravec, R., Conger, K.K., D'Souza, R., Allison, A.B., and Casanova, J.E. (2012). BRAG2/GEP100/IQSec1 interacts with clathrin and regulates α5β1 integrin endocytosis through activation of ADP ribosylation factor 5 (Arf5). J. Biol. Chem. 287, 31138–31147.

Murthy, M., Garza, D., Scheller, R.H., and Schwarz, T.L. (2003). Mutations in the exocyst component Sec5 disrupt neuronal membrane traffic, but neurotransmitter release persists. Neuron 37, 433–447.

Nakai, W., Kondo, Y., Saitoh, A., Naito, T., Nakayama, K., and Shin, H.-W. (2013). ARF1 and ARF4 regulate recycling endosomal morphology and retrograde transport from endosomes to the Golgi apparatus. Mol. Biol. Cell 24, 2570–2581.

Neidert, A.H., Virupannavar, V., Hooker, G.W., and Langeland, J.A. (2001). Lamprey Dlx

genes and early vertebrate evolution. Proc. Natl. Acad. Sci. U. S. A. 98, 1665.

Nicolas, L.B., Kolb, Y., and Prinssen, E.P. (2006). A combined marble burying-locomotor activity test in mice: a practical screening test with sensitivity to different classes of anxiolytics and antidepressants. Eur. J. Pharmacol. 547, 106–115.

Obenauer, J.C. (2003). Scansite 2.0: proteome-wide prediction of cell signaling interactions using short sequence motifs. Nucleic Acids Res. 31, 3635–3641.

Obholzer, N., Wolfson, S., Trapani, J.G., Mo, W., Nechiporuk, A., Busch-Nentwich, E., Seiler, C., Sidi, S., S\öllner, C., Duncan, R.N., Boehland, A., Nicolson, T. (2008). Vesicular glutamate transporter 3 is required for synaptic transmission in zebrafish hair cells. J. Neurosci. 28, 2110.

Oh, A.K. (2013). Genetics of vestibulopathy and migraine. Curr. Opin. Otolaryngol. Head Neck Surg. 21, 469–472.

Paffenholz, R., Bergstrom, R.A., Pasutto, F., Wabnitz, P., Munroe, R.J., Jagla, W., Heinzmann, U., Marquardt, A., Bareiss, A., Laufs, J., Russ, A., Stumm, G., Schimenti, J.C., Bergstrom, D.E. (2004). Vestibular defects in head-tilt mice result from mutations in Nox3, encoding an NADPH oxidase. Genes Dev. 18, 486–491.

Pagni, M., Ioannidis, V., Cerutti, L., Zahn-Zabal, M., Jongeneel, C.V., Hau, J., Martin, O., Kuznetsov, D., and Falquet, L. (2007). MyHits: improvements to an interactive resource for analyzing protein sequences. Nucleic Acids Res. 35, W433–7.

Pan, N., Jahan, I., Kersigo, J., Kopecky, B., Santi, P., Johnson, S., Schmitz, H., and Fritzsch, B. (2011). Conditional deletion of Atoh1 using Pax2-Cre results in viable mice without differentiated cochlear hair cells that have lost most of the organ of Corti. Hear. Res. 275, 66–80.

Patterson, R. a, Juarez, M.T., Hermann, A., Sasik, R., Hardiman, G., and McGinnis, W. (2013). Serine proteolytic pathway activation reveals an expanded ensemble of wound response genes in Drosophila. PLoS One 8, e61773.

Pauley, S., Lai, E., and Fritzsch, B. (2006). Foxg1 is required for morphogenesis and histogenesis of the mammalian inner ear. Dev. Dyn. 235, 2470–2482.

Petko, J.A., Kabbani, N., Frey, C., Woll, M., Hickey, K., Craig, M., Canfield, V.A., and Levenson, R. (2009). Proteomic and functional analysis of NCS-1 binding proteins reveals novel signaling pathways required for inner ear development in zebrafish. BMC Neurosci. 10, 27.

Le Pichon, C.E., Valley, M.T., Polymenidou, M., Chesler, A.T., Sagdullaev, B.T., Aguzzi, A., and Firestein, S. (2008). Olfactory behavior and physiology are disrupted in prion protein knockout mice. Nat. Neurosci. 12, 60–69.

Pond, S.L.K., and Frost, S.D.W. (2010). Datamonkey: rapid detection of selective pressure on individual sites of codon alignments. Bioinformatics 21, 2531 –2533.

Pond, S.L.K., Frost, S.D.W., and Muse, S. V (2005). HyPhy: hypothesis testing using phylogenies. Bioinformatics 21, 676–679.

Popko, B., Puckett, C., Lai, E., Shine, H.D., Readhead, C., Takahashi, N., Hunt, S.W., Sidman, R.L., and Hood, L. (1987). Myelin deficient mice: expression of myelin basic protein and generation of mice with varying levels of myelin. Cell 48, 713–721.

Preitner, N., Damiola, F., Zakany, J., Duboule, D., Albrecht, U., and Schibler, U. (2002). The Orphan Nuclear Receptor REV-ERBα Controls Circadian Transcription within the Positive Limb of the Mammalian Circadian Oscillator. Cell 110, 251–260.

Purves, D., Augustine, G., Fitzpatrick, D., Hall, W., LaManitia, A., McNamara, J., and White, L. (2008). Neuroscience (Sinauer Associates Inc).

Quevillon, E., Silventoinen, V., Pillai, S., Harte, N., Mulder, N., Apweiler, R., and Lopez, R. (2005). InterProScan: protein domains identifier. Nucleic Acids Res. 33, W116–20.

Riccomagno, M.M., Takada, S., and Epstein, D.J. (2005). Wnt-dependent regulation of inner ear morphogenesis is balanced by the opposing and supporting roles of Shh. Genes Dev. 19, 1612–1623.

Richardson, M.K., Admiraal, J., and Wright, G.M. (2010). Developmental anatomy of lampreys. Biol. Rev. Camb. Philos. Soc. 85, 1–33.

Robles, M.S., Cox, J., and Mann, M. (2014). In-vivo quantitative proteomics reveals a key contribution of post-transcriptional mechanisms to the circadian regulation of liver metabolism. PLoS Genet. 10, e1004047.

Sadakata, T., Shinoda, Y., Sekine, Y., Saruta, C., Itakura, M., Takahashi, M., and Furuichi, T. (2010). Interaction of calcium-dependent activator protein for secretion 1 (CAPS1) with the class II ADP-ribosylation factor small GTPases is required for dense-core vesicle trafficking in the trans-Golgi network. J. Biol. Chem. 285, 38710–38719.

Shigeyoshi, Y., Taguchi, K., Yamamoto, S., Takekida, S., Yan, L., Tei, H., Moriya, T., Shibata, S., Loros, J.J., Dunlap, J.C., Okamura, H. (1997). Light-induced resetting of a mammalian circadian clock is associated with rapid induction of the mPer1 transcript. Cell 91, 1043–1053.

Sigrist, C.J. a, de Castro, E., Cerutti, L., Cuche, B. a, Hulo, N., Bridge, A., Bougueleret, L., and Xenarios, I. (2013). New and continuing developments at PROSITE. Nucleic Acids Res. 41, D344–7.

Simon, A.L., Stone, E.A., and Sidow, A. (2002). Inference of functional regions in proteins by quantification of evolutionary constraints. Proc. Natl. Acad. Sci. U. S. A. 99, 2912.

Skoff, R. (1976). Myelin deficit in the Jimpy mouse may be due to cellular abnormalities in astroglia. Nature 264, 560–562.

Stearns, T., Willingham, M.C., Botstein, D., and Kahn, R.A. (1990). ADP-ribosylation factor is functionally and physically associated with the Golgi complex. Proc. Natl. Acad. Sci. U. S. A. 87, 1238–1242.

Stettler, D.D., and Axel, R. (2009). Representations of odor in the piriform cortex. Neuron 63, 854–864.

Stevens, C.B., Davies, A.L., Battista, S., Lewis, J.H., and Fekete, D.M. (2003). Forced activation of Wnt signaling alters morphogenesis and sensory organ identity in the chicken inner ear. Dev. Biol. 261, 149–164.

Sumantra, C., Petra, K., and Thomas, L. (2010). A symphony of inner ear developmental control genes. BMC Genet. 11, 68–68.

Suter, U., Welcher, A.A., Özcelik, T., Snipes, G.J., Kosaras, B., Francke, U., Billings-Gagliardi, S., Sidman, R.L., and Shooter, E.M. (1992). Trembler mouse carries a point mutation in a myelin gene. Nature 356, 241–243.

Taglialatela, P., Soria, J.M., Caironi, V., Moiana, A., and Bertuzzi, S. (2004). Compromised generation of GABAergic interneurons in the brains of Vax1-/- mice. Development 131, 4239 –4249.

Takatsu, H., Yoshino, K., Toda, K., and Nakayama, K. (2002). GGA proteins associate with Golgi membranes through interaction between their GGAH domains and ADP-ribosylation factors. Biochem. J. 365, 369–378.

Tascioglu, A. (2005). Brief review of vestibular system anatomy and its higher order projections. Neuroanatomy 4, 24–27.

Thisse, B., Pflumio, S., Fürthauer, M., Loppin, B., Heyer, V., Degrave, A., Woehl, R., Lux, A., Steffan, T., Charbonnier, X.Q., Thisse, C. (2001). Expression of the zebrafish genome during embryogenesis.

Vela, J.M., Gonzalez, B., and Castellano, B. (1998). Understanding glial abnormalities associated with myelin deficiency in the jimpy mutant mouse. Brain Res. Rev. 26, 29–42.

Vrijens, K., Thys, S., De Jeu, M.T., Postnov, A.A., Pfister, M., Cox, L., Zwijsen, A., Van Hoof, V., Mueller, M., De Clerck, N.M., De Zeeuw, C.I., Van Camp, G., Van Laer, L. (2006). Ozzy, a Jag1 vestibular mouse mutant, displays characteristics of Alagille syndrome. Neurobiol. Dis. 24, 28–40.

Wang, H., Yang, H., Shivalila, C.S., Dawlaty, M.M., Cheng, A.W., Zhang, F., and Jaenisch, R. (2013). One-Step Generation of Mice Carrying Mutations in Multiple Genes by CRISPR/Cas-Mediated Genome Engineering. Cell 153, 910–918.

Wang, X., Dellamary, L., Fernandez, R., Harrop, A., Keithley, E.M., Harris, J.P., Ye, Q., Lichter, J., LeBel, C., and Piu, F. (2009). Dose-dependent sustained release of dexamethasone in inner ear cochlear fluids using a novel local delivery approach. Audiol. Neurootol. 14, 393–401.

Watson, G.M., Graugnard, E.M., and Mire, P. (2007). The involvement of arl-5b in the repair of hair cells in sea anemones. J. Assoc. Res. Otolaryngol. 8, 183–193.

Weimar, W.R., Lane, P.W., and Sidman, R.L. (1982). Vibrator (vb): a spinocerebellar system degeneration with autosomal recessive inheritance in mice. Brain Res. 251, 357–364.

Wilson, D.A., and Stevenson, R.J. (2003). The fundamental role of memory in olfactory perception. Trends Neurosci. 26, 243–247.

Yang, M., and Crawley, J.N. (2009). Simple Behavioral Assessment of Mouse Olfaction. J.N. Crawley, C.R. Gerfen, M.A. Rogawski, D.R. Sibley, P. Skolnick, and S. Wray, eds. (Hoboken, NJ, USA: John Wiley & Sons, Inc.).

Yi, C., Scherer, T., Tschop, M. (2011). Cajal revisited: does the VMH make us fat?Nature Neuroscience. 14, 806-808.

Zallocchi, M., Delimont, D., Meehan, D.T., and Cosgrove, D. (2012). Regulated vesicular trafficking of specific PCDH15 and VLGR1 variants in auditory hair cells. J. Neurosci. 32, 13841–13859.

Zhang, E.E., and Kay, S.A. (2010). Clocks not winding down: unravelling circadian networks. Nat. Rev. Mol. Cell Biol. 11, 764–776.

Zhang, W., Yan, Z., Jan, L.Y., and Jan, Y.N. (2013). Sound response mediated by the TRP channels NOMPC, NANCHUNG, and INACTIVE in chordotonal organs of Drosophila larvae. Proc. Natl. Acad. Sci. U. S. A. 110, 13612–13617.

Zheng, B.H., Larkin, D.W., Albrecht, U., Sun, Z.S., Sage, M., Eichele, G., Lee, C.C., and Bradley, A. (1999). The mPer2 gene encodes a functional component of the mammalian

circadian clock. Nature 400, 169–173.

Zheng, L., Sekerková, G., Vranich, K., Tilney, L.G., Mugnaini, E., and Bartles, J.R. (2010). The deaf Jerker mouse has a mutation in the gene encoding the espin actin-bundling proteins of hair cell stereocilia and fails to accumulate Espins. Cell 102, 377–385.

Zingler, V.C., Weintz, E., Jahn, K., Huppert, D., Cnyrim, C., Brandt, T., and Strupp, M. (2009). Causative Factors, Epidemiology, and Follow-up of Bilateral Vestibulopathy. In Annals of the New York Academy of Sciences, (Blackwell Publishing), pp. 505–508.